

# Dynamic stiffness matrix based on the extended separation-of-variables solution for the free vibration of orthotropic rectangular thin plates

Shiyi Mei<sup>a</sup>, Colin Caprani<sup>a,\*</sup>, Daniel Cantero<sup>b</sup>

<sup>a</sup>*Department of Civil Engineering, Monash University, Melbourne, Victoria, Australia*

<sup>b</sup>*Department of Structural Engineering, Norwegian University of Science & Technology NTNU, Trondheim, Norway*

---

## Abstract

The dynamic stiffness matrix (DSM) based on the extended separation-of-variables (SOV) solution is developed for the free vibration analysis of an orthotropic rectangular thin plate with general homogeneous boundary conditions. The method combines the advantages of the DSM method and the SOV method. The SOV solution satisfies the governing differential equation derived from Rayleigh's principle and is used to formulate dynamic stiffness matrices. Owing to the characteristics of the SOV solution, the fully clamped boundary condition problem associated with the Wittrick–Williams algorithm is resolved. The enhanced algorithm is further proposed to solve dynamic stiffness matrices, rather than solving eigenvalue equations. A numerical technique for mode shape computation is also introduced. The accuracy of the proposed method is validated through numerical experiments.

---

## 1. Introduction

Rectangular plates play an important role in various engineering fields, including civil, mechanical, and aerospace engineering [3]. The free vibration of plates has been a fundamental research problem for over two centuries. The earliest exact solutions for this problem are the Navier [21] and Levy

---

\*Corresponding author

*Email addresses:* shiyi.mei1@monash.edu (Shiyi Mei), colin.caprani@monash.edu (Colin Caprani), daniel.cantero@ntnu.no (Daniel Cantero)

6 [14] solutions, which require at least one pair of opposite edges to be simply  
 7 supported or guided. To solve problems with other boundary conditions, ap-  
 8 proximate solutions such as the Rayleigh–Ritz method [13] and the Galerkin  
 9 method [12] have been widely applied. For these approximation methods,  
 10 beam functions, polynomials, trigonometric functions, and their combina-  
 11 tions [16] are commonly used as the assumed approximate functions. The  
 12 accuracy of these solutions depends on how well the assumed approximate  
 13 functions represent the displacement of the plate.

14 Besides the approximation methods, several analytical methods have been  
 15 developed over past decades, including the Kantorovich-Krylov method [9,  
 16 10], the symplectic eigenfunction expansion method [32, 25], the separation-  
 17 of-variable (SOV) method [29], the dynamic stiffness matrix (DSM) method  
 18 [2], and series expansion-based methods [24]. The series expansion-based  
 19 methods include the superposition method [22, 7], Fourier series method  
 20 [11, 17], the finite integral transform method [15, 33], and other series meth-  
 21 ods. These methods represent the plate displacement in terms of an infinite  
 22 series and mostly are capable of handling any general boundary conditions.  
 23 However, sufficient truncation of the series is required to ensure the accuracy  
 24 and convergence of the results, and the eigenvalue equation is generally dif-  
 25 ficult to express explicitly. Therefore, solving the corresponding eigenvalue  
 26 problem can be computationally expensive.

27 Despite being a powerful method for the dynamic analysis of plate as-  
 28 semblies, the finite element method (FEM) requires a sufficient number of  
 29 elements and is computationally expensive to accurately capture higher-order  
 30 modes. Thus, the DSM method was developed as an accurate and efficient  
 31 analytical approach to alternatively solve complex plate structures [4, 5]. The  
 32 DSM can be considered as an analytical FEM since the mode functions of  
 33 the plate are expressed by analytical solutions, where Levy-type solution [6]  
 34 or components of infinite Fourier series [1, 19] are applied. To avoid solving  
 35 the cumbersome transcendental frequency equation directly, the Wittrick-  
 36 Williams (W-W) algorithm [23] is applied to the eigenvalue problem. The  
 37 W-W algorithm determines the lower and upper bounds of natural frequen-  
 38 cies to arbitrary precision rather than solving the frequency equation directly.  
 39 Thus, the DSM has the potential to be effectively and systematically solved  
 40 using the W-W algorithm. However, a critical part in applying the W-W  
 41 algorithm is to determine all natural frequencies of the fully clamped struc-  
 42 ture within the interested frequency range, *a priori*. Strategies such as using  
 43 a sufficiently fine mesh or including a sufficient number of terms in series

expansions [1] can ensure that all fully clamped frequencies are accounted for, thereby maintaining the accuracy of the algorithm. However, these approaches are computationally expensive and complex, posing a significant obstacle to the wider adoption and application of the DSM method based on the W-W algorithm [8]. To resolve the fully clamped plate problem, Liu and Banerjee [18] suggested that the frequencies can be indirectly obtained from the simply supported plate problem, where the Navier solution serves as the analytical solution. This provides a significant enhancement to the W-W algorithm, increasing the efficiency of applying DSM methods. However, the solutions are not explicit and closed-form, but are expressed in an infinite series form, where a sufficient number of truncation terms is required to ensure accuracy.

Inspired by the Navier and Levy solutions, Xing and Liu [29] proposed the SOV method, which provides concise and explicit eigensolutions. The mode shape function has a separable form,  $\phi(x)\psi(y)$ , requiring only one  $\phi(x)$  and one  $\psi(y)$  for each mode order, allowing each eigenvalue equation to be explicitly expressed. However, this SOV method is not suitable to deal with plates with free boundary conditions. Therefore, an extended SOV method [26, 27] based on the Rayleigh quotient was proposed to accommodate plates with all four classical boundary conditions, i.e., simply supported, clamped, guided, and free. Based on the Rayleigh quotient model, alternative iterative and improved SOV methods have been subsequently proposed [28]. Although SOV methods provide concise closed-form analytical solutions, they require solving a specific set of highly nonlinear eigenvalue equations for each type of boundary condition. However, even when considering only the four classic homogeneous cases, it becomes evident that 55 different boundary condition combinations exist for a rectangular plate, making the process tedious.

In this study, the SOV method is further extended to analyze the vibrations of plates with elastically restrained edges. This extended SOV solution is then employed to construct dynamic stiffness matrices, which accommodate all general homogeneous boundary conditions. By taking advantage of both the SOV and DSM methods, an enhanced W-W algorithm is developed to solve the eigenvalue problem without directly solving the eigenvalue equations. This enhanced approach resolves the challenge of determining fully clamped frequencies, a well-known limitation in the application of the W-W algorithm. In addition, a novel numerical technique is proposed to compute the mode shape coefficients.

## 81 2. Mathematical model

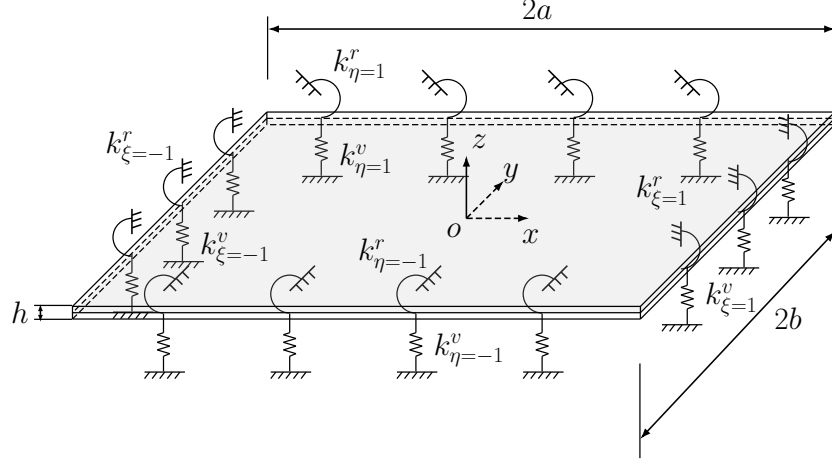


Figure 1: The orthotropic rectangular plate with all edges elastically restrained.

82 Consider a thin orthotropic rectangular plate of length  $2a$  and width  
 83  $2b$ , with all four edges restrained by vertical translational springs  $k^v$  and  
 84 rotational springs  $k^r$ , as shown in Figure 1. The coordinate origin is located  
 85 at the center of the plate.

86 The governing differential equation for the free vibration of a thin or-  
 87 thotropic plate is given by [28]:

$$D_{11} \frac{\partial^4 w}{\partial \xi^4} + 2D_3 \chi^2 \frac{\partial^4 w}{\partial \xi^2 \partial \eta^2} + D_{22} \chi^4 \frac{\partial^4 w}{\partial \eta^4} = \rho h a^4 \omega^2 w, \quad (1)$$

88 where  $\chi = a/b$  is the aspect ratio;  $\xi = x/a$  and  $\eta = y/b$  are the normalized  
 89 coordinates, and the bending stiffness parameters are defined as:

$$\begin{aligned} D_{11} &= \frac{E_1 h^3}{12(1 - v_{12}v_{21})}, & D_{22} &= \frac{E_2 h^3}{12(1 - v_{12}v_{21})}, \\ D_{66} &= \frac{G_{12} h^3}{12}, & D_{12} &= v_{12}D_{22} = v_{21}D_{11}, & D_3 &= D_{12} + 2D_{66}, \end{aligned} \quad (2)$$

90 where  $\rho$  and  $h$  denote the mass density and thickness of the plate, respec-  
 91 tively;  $E_1$  and  $E_2$  are the Young's moduli in the  $x$ - and  $y$ -directions, respec-  
 92 tively;  $G_{12}$  is the shear modulus, and  $v_{12}$  and  $v_{21}$  are the Poisson's ratios.

93 Instead of solving the free vibration of the thin orthotropic plate using  
 94 Equation (1), it is suggested that the vibration of the thin plate can also be  
 95 solved using the Rayleigh quotient variational principle [26]:

$$\delta U = \delta T, \quad (3)$$

96 where  $\delta$  denotes variation,  $U$  is the magnitude of the potential energy of the  
 97 plate, and  $T$  represents the magnitude of the kinetic energy of the plate. The  
 98 potential energy of the plate can be expressed as [27]:

$$U^I = \frac{1}{2} \iint \left[ D_{11} \left( \frac{\partial^2 W}{\partial x^2} \right)^2 + 2D_{12} \frac{\partial^2 W}{\partial x^2} \frac{\partial^2 W}{\partial y^2} + D_{22} \left( \frac{\partial^2 W}{\partial y^2} \right)^2 \right. \\ \left. + 4D_{66} \left( \frac{\partial^2 W}{\partial x \partial y} \right)^2 \right] dx dy. \quad (4)$$

99 And the kinetic energy is:

$$T = \frac{1}{2} \iint \rho h \left( \frac{\partial W}{\partial t} \right)^2 dx dy. \quad (5)$$

100 Assuming the solution of the deflection  $W(x, y; t) = w(x, y)e^{i\omega t}$  for har-  
 101 monic plate motion, where  $i = \sqrt{-1}$ ,  $w(x, y)$  is the mode shape, and  $\omega$  is the  
 102 radial frequency. By substituting  $W(x, y; t) = w(x, y)e^{i\omega t}$  into Equations (4)  
 103 and (5) and expressing the system in dimensionless coordinates, we have:

$$U^I = \frac{ab}{2} \iint \left[ \frac{D_{11}}{a^4} \left( \frac{\partial^2 w}{\partial \xi^2} \right)^2 + \frac{2D_{12}}{a^2 b^2} \frac{\partial^2 w}{\partial \xi^2} \frac{\partial^2 w}{\partial \eta^2} + \frac{D_{22}}{b^4} \left( \frac{\partial^2 w}{\partial \eta^2} \right)^2 \right. \\ \left. + \frac{4D_{66}}{a^2 b^2} \left( \frac{\partial^2 w}{\partial \xi \partial \eta} \right)^2 \right] d\xi d\eta, \quad (6)$$

104 and

$$T = \omega^2 \frac{ab}{2} \rho h \iint w^2 d\xi d\eta = \omega^2 T_0, \quad (7)$$

105 where,  $T_0$  is defined as the coefficient of the kinetic energy.

106 The separable form of the mode shape function  $w(\xi, \eta)$  is given by:

$$w(\xi, \eta) = \phi(\xi)\psi(\eta), \quad (8)$$

107 where  $\phi(\xi)$  and  $\psi(\eta)$  can be expressed as:

$$\phi(\xi) = A_1 \sin(\alpha_1 \xi) + A_2 \cos(\alpha_1 \xi) + A_3 \sinh(\beta_1 \xi) + A_4 \cosh(\beta_1 \xi), \quad (9a)$$

$$\psi(\eta) = B_1 \sin(\alpha_2 \eta) + B_2 \cos(\alpha_2 \eta) + B_3 \sinh(\beta_2 \eta) + B_4 \cosh(\beta_2 \eta). \quad (9b)$$

108 Based on Equation (3), the frequencies  $\omega_x$  and  $\omega_y$ , corresponding to the  
 109 mode shapes  $\phi(\xi)$  and  $\psi(\eta)$ , respectively, are assumed to be independent of  
 110 each other. This is a common and important assumption in SOV methods,  
 111 and  $\omega_x$  and  $\omega_y$  can be different in a mathematical sense [27].

### 112 2.1. Dynamic stiffness matrix corresponding to $\omega_x$

113 For given general homogeneous boundary conditions, we can first assume  
 114 that the mode shape  $\psi(\eta)$  corresponding to the  $y$ -direction is known. Sup-  
 115 posing the edges of the plate in both the  $x$ - and  $y$ -directions are elastically  
 116 restrained by homogeneous vertical translational and rotational springs. The  
 117 vertical translational and rotational springs at the  $\xi = -1$  end are denoted  
 118 as  $k_{\xi=-1}^v$  and  $k_{\xi=-1}^r$ , respectively, and at the  $\xi = 1$  end as  $k_{\xi=1}^v$  and  $k_{\xi=1}^r$ ,  
 119 respectively. Thus, the potential energy along the supported edge in the  
 120  $x$ -direction can be expressed by:

$$\begin{aligned} U^x = & \int \left[ k_{\xi=-1}^r \left( \frac{\partial W}{\partial x} \right)^2 + k_{\xi=-1}^v (W)^2 \right]_{x=-a} dy \\ & + \int \left[ k_{\xi=1}^r \left( \frac{\partial W}{\partial x} \right)^2 + k_{\xi=1}^v (W)^2 \right]_{x=a} dy. \end{aligned} \quad (10)$$

121 From Equation (10), the magnitude of potential energy along the plate edges  
 122 in the  $x$ -direction, expressed in dimensionless coordinates, is obtained as:

$$\begin{aligned} U^x = & ab \int \left[ \frac{k_{\xi=-1}^r}{a^3} \left( \frac{\partial w}{\partial \xi} \right)^2 + \frac{k_{\xi=-1}^v}{a} (w)^2 \right]_{\xi=-1} d\eta \\ & + ab \int \left[ \frac{k_{\xi=1}^r}{a^3} \left( \frac{\partial w}{\partial \xi} \right)^2 + \frac{k_{\xi=1}^v}{a} (w)^2 \right]_{\xi=1} d\eta. \end{aligned} \quad (11)$$

123 The magnitude of total potential energy of the plate in the  $x$ -direction can  
 124 be obtained from Equations (6) and (11) as:

$$\begin{aligned}
 U &= U^I + U^x \\
 &= \frac{ab}{2} \iint \left[ \frac{D_{11}}{a^4} \left( \frac{\partial^2 w}{\partial \xi^2} \right)^2 + \frac{2D_{12}}{a^2 b^2} \frac{\partial^2 w}{\partial \xi^2} \frac{\partial^2 w}{\partial \eta^2} + \frac{D_{22}}{b^4} \left( \frac{\partial^2 w}{\partial \eta^2} \right)^2 \right. \\
 &\quad \left. + \frac{4D_{66}}{a^2 b^2} \left( \frac{\partial^2 w}{\partial \xi \partial \eta} \right)^2 \right] d\xi d\eta \\
 &\quad + ab \int \left[ \frac{k_{\xi=1}^r}{a^3} \left( \frac{\partial w}{\partial \xi} \right)^2 + \frac{k_{\xi=1}^v}{a} (w)^2 \right]_{\xi=1} d\eta \\
 &\quad + ab \int \left[ \frac{k_{\xi=-1}^r}{a^3} \left( \frac{\partial w}{\partial \xi} \right)^2 + \frac{k_{\xi=-1}^v}{a} (w)^2 \right]_{\xi=-1} d\eta
 \end{aligned} \tag{12}$$

125 By substituting Equation (8) into Equation (12), we have:

$$\begin{aligned}
 U &= \frac{ab}{2} \int_{-1}^1 \left[ \frac{D_{11}}{a^4} I_1 \left( \frac{d^2 \phi}{d\xi^2} \right)^2 + \frac{2D_{12}}{a^2 b^2} I_2 \frac{d^2 \phi}{d\xi^2} \phi + \frac{D_{22}}{b^4} I_4 \phi^2 \right. \\
 &\quad \left. + \frac{4D_{66}}{a^2 b^2} I_3 \left( \frac{d\phi}{d\xi} \right)^2 \right] d\xi \\
 &\quad + ab I_1 \left[ \frac{k_{\xi=-1}^r}{a^3} \left( \frac{d\phi}{d\xi} \right)^2 + \frac{k_{\xi=-1}^v}{a} (\phi)^2 \right]_{\xi=-1} \\
 &\quad + ab I_1 \left[ \frac{k_{\xi=1}^r}{a^3} \left( \frac{d\phi}{d\xi} \right)^2 + \frac{k_{\xi=1}^v}{a} (\phi)^2 \right]_{\xi=1},
 \end{aligned} \tag{13}$$

126 where the integral parameters  $I_1$ ,  $I_2$ ,  $I_3$ , and  $I_4$  are defined and expressed in  
 127 Appendix A.

128 By taking Equation (8) into account, the coefficient  $T_0$  of the kinetic  
 129 energy from Equation (7) for the plate in the  $x$ -direction can be expressed  
 130 as:

$$T_0 = \frac{ab}{2} \rho h \iint w^2 d\xi d\eta = \frac{ab}{2} \rho h I_1 \int_{-1}^1 \phi^2 d\xi. \tag{14}$$

131 Taking the Rayleigh principle in the form:

$$\delta U = \omega_x^2 \delta T_0, \tag{15}$$

and by substituting Equations (13) and (14) into Equation (15), and relieving  $\delta\phi$  and  $\delta\frac{d\phi}{d\xi}$  in Equation (15) by calculus of variations, yields:

$$\begin{aligned}
0 = & \int_{-1}^1 \left[ \frac{D_{11}}{a^4} I_1 \frac{d^4\phi}{d\xi^4} + \left( \frac{2D_{12}}{a^2b^2} I_2 - \frac{4D_{66}}{a^2b^2} I_3 \right) \frac{d^2\phi}{d\xi^2} \right. \\
& + \left. \left( \frac{D_{22}}{b^4} I_4 - \omega_x^2 \rho h I_1 \right) \phi \right] \delta\phi d\xi \\
& + \frac{2k_{\xi=-1}^v}{a} I_1 (\phi \delta\phi)_{\xi=-1} + \frac{2k_{\xi=1}^v}{a} I_1 (\phi \delta\phi)_{\xi=1} \\
& + \left[ \left( \frac{4D_{66}}{a^2b^2} I_3 - \frac{D_{12}}{a^2b^2} I_2 \right) \frac{d\phi}{d\xi} - \frac{D_{11}}{a^4} I_1 \frac{d^3\phi}{d\xi^3} \right] \delta\phi \Big|_{\xi=-1}^{\xi=1} \\
& + \left( \frac{D_{12}}{a^2b^2} I_2 \phi + \frac{D_{11}}{a^4} I_1 \frac{d^2\phi}{d\xi^2} \right) \delta \frac{d\phi}{d\xi} \Big|_{\xi=-1}^{\xi=1} \\
& + \frac{2k_{\xi=-1}^r}{a^3} I_1 \left( \frac{d\phi}{d\xi} \delta \frac{d\phi}{d\xi} \right)_{\xi=-1} + \frac{2k_{\xi=1}^r}{a^3} I_1 \left( \frac{d\phi}{d\xi} \delta \frac{d\phi}{d\xi} \right)_{\xi=1}.
\end{aligned} \tag{16}$$

Thus, the governing differential equation in the  $x$ -direction can be obtained from the integration part in Equation (16):

$$\frac{d^4\phi}{d\xi^4} + 2\chi^2 \left( \frac{D_{12}I_2}{D_{11}I_1} - 2\frac{D_{66}I_3}{D_{11}I_1} \right) \frac{d^2\phi}{d\xi^2} + \left( \chi^4 \frac{D_{22}I_4}{D_{11}I_1} - a^4 \Omega_x^4 \right) \phi = 0, \tag{17}$$

where  $\Omega_x = \sqrt[4]{\omega_x^2 \rho h / D_{11}}$ . By substituting  $\phi(\xi) = Ae^{\mu\xi}$  into Equation (17), we obtain:

$$\mu^4 + 2\chi^2 \left( \frac{D_{12}I_2}{D_{11}I_1} - 2\frac{D_{66}I_3}{D_{11}I_1} \right) \mu^2 + \left( \chi^4 \frac{D_{22}I_4}{D_{11}I_1} - a^4 \Omega_x^4 \right) = 0. \tag{18}$$

And so the solution for  $\mu$  can be expressed as:

$$\mu_{1,2} = \pm i\alpha_1, \quad \mu_{3,4} = \pm \beta_1, \tag{19}$$

where,

$$\alpha_1 = \chi \sqrt{\sqrt{\left( \frac{D_{12}I_2}{D_{11}I_1} - 2\frac{D_{66}I_3}{D_{11}I_1} \right)^2 - \frac{D_{22}I_4}{D_{11}I_1} + b^4 \Omega_x^4} + \frac{D_{12}I_2}{D_{11}I_1} - 2\frac{D_{66}I_3}{D_{11}I_1}}, \tag{20a}$$

$$\beta_1 = \chi \sqrt{\sqrt{\left( \frac{D_{12}I_2}{D_{11}I_1} - 2\frac{D_{66}I_3}{D_{11}I_1} \right)^2 - \frac{D_{22}I_4}{D_{11}I_1} + b^4 \Omega_x^4} - \frac{D_{12}I_2}{D_{11}I_1} + 2\frac{D_{66}I_3}{D_{11}I_1}}. \tag{20b}$$



140 The boundary conditions along the edges in the  $x$ -direction can be obtained  
 141 from the remaining  $\delta\phi$  and  $\delta\frac{d\phi}{d\xi}$  parts in Equation (16). The shear force  
 142 equilibrium can be obtained from the  $\delta\phi$  part:

$$\begin{aligned} & \left[ \left( \frac{4D_{66}}{a^2b^2} I_3 - \frac{D_{12}}{a^2b^2} I_2 \right) \frac{d\phi}{d\xi} - \frac{D_{11}}{a^4} I_1 \frac{d^3\phi}{d\xi^3} \right] \Big|_{\xi=-1}^{\xi=1} \\ & + \frac{2k_{\xi=-1}^v}{a} I_1 (\phi)_{\xi=-1} + \frac{2k_{\xi=1}^v}{a} I_1 (\phi)_{\xi=1} = 0, \end{aligned} \quad (21)$$

143 and from the  $\delta\frac{d\phi}{d\xi}$  part, the bending moment equilibrium:

$$\begin{aligned} & \left( \frac{D_{12}}{a^2b^2} I_2 \phi + \frac{D_{11}}{a^4} I_1 \frac{\partial^2 \phi}{\partial \xi^2} \right) \Big|_{\xi=-1}^{\xi=1} \\ & + \frac{2k_{\xi=-1}^r}{a^3} I_1 \left( \frac{\partial \phi}{\partial \xi} \right)_{\xi=-1} + \frac{2k_{\xi=1}^r}{a^3} I_1 \left( \frac{\partial \phi}{\partial \xi} \right)_{\xi=1} = 0. \end{aligned} \quad (22)$$

144 Thus, we can obtain the shear force and bending moment equilibrium along  
 145 the edges  $\xi = -1$  and  $\xi = 1$  from Equations (21) and (22), respectively, as:

$$\frac{d^3\phi}{d\xi^3} - \chi^2 \left( \frac{4D_{66}I_3}{D_{11}I_1} - \frac{D_{12}I_2}{D_{11}I_1} \right) \frac{d\phi}{d\xi} + \frac{2a^3k_{\xi=-1}^v}{D_{11}} \phi = 0, \quad \xi = -1, \quad (23a)$$

$$\frac{d^2\phi}{d\xi^2} + \frac{\chi^2 D_{12}I_2}{D_{11}I_1} \phi - \frac{2ak_{\xi=-1}^r}{D_{11}} \frac{d\phi}{d\xi} = 0, \quad \xi = -1, \quad (23b)$$

$$\frac{d^3\phi}{d\xi^3} - \chi^2 \left( \frac{4D_{66}I_3}{D_{11}I_1} - \frac{D_{12}I_2}{D_{11}I_1} \right) \frac{d\phi}{d\xi} - \frac{2a^3k_{\xi=1}^v}{D_{11}} \phi = 0, \quad \xi = 1, \quad (23c)$$

$$\frac{d^2\phi}{d\xi^2} + \frac{\chi^2 D_{12}I_2}{D_{11}I_1} \phi + \frac{2ak_{\xi=1}^r}{D_{11}} \frac{d\phi}{d\xi} = 0, \quad \xi = 1. \quad (23d)$$

146 Substituting Equation (9a) into Equation (23), and denoting  $k_{\xi}^{v*} = \frac{2a^3k_{\xi}^v}{D_{11}}$ ,  
 147  $k_{\eta}^{r*} = \frac{2ak_{\eta}^r}{D_{11}}$ ,  $S_{\alpha_1} = \sin \alpha_1$ ,  $C_{\alpha_1} = \cos \alpha_1$ ,  $Sh_{\beta_1} = \sinh \beta_1$ , and  $Ch_{\beta_1} = \cosh \beta_1$ ,

148 we have:

$$\begin{bmatrix} \gamma_1 C_{\alpha_1} - k_{\xi=-1}^{v*} S_{\alpha_1} & \gamma_1 S_{\alpha_1} + k_{\xi=-1}^{v*} C_{\alpha_1} & \gamma_2 Ch_{\beta_1} - k_{\xi=-1}^{v*} Sh_{\beta_1} \\ \gamma_3 S_{\alpha_1} + k_{\xi=-1}^{r*} \alpha_1 C_{\alpha_1} & -\gamma_3 C_{\alpha_1} + k_{\xi=-1}^{r*} \alpha_1 S_{\alpha_1} & \gamma_4 Sh_{\beta_1} + k_{\xi=-1}^{r*} \beta_1 Ch_{\beta_1} \\ -\gamma_1 C_{\alpha_1} + k_{\xi=1}^{v*} S_{\alpha_1} & \gamma_1 S_{\alpha_1} + k_{\xi=1}^{v*} C_{\alpha_1} & -\gamma_2 Ch_{\beta_1} + k_{\xi=1}^{v*} Sh_{\beta_1} \\ \gamma_3 S_{\alpha_1} + k_{\xi=1}^{r*} \alpha_1 C_{\alpha_1} & \gamma_3 C_{\alpha_1} - k_{\xi=1}^{r*} \alpha_1 S_{\alpha_1} & \gamma_4 Sh_{\beta_1} + k_{\xi=1}^{r*} \beta_1 Ch_{\beta_1} \\ -\gamma_2 Sh_{\beta_1} + k_{\xi=-1}^{v*} Ch_{\beta_1} \\ -\gamma_4 Ch_{\beta_1} - k_{\xi=-1}^{r*} \beta_1 Sh_{\beta_1} \\ -\gamma_2 Sh_{\beta_1} + k_{\xi=1}^{v*} Ch_{\beta_1} \\ \gamma_4 Ch_{\beta_1} + k_{\xi=1}^{r*} \beta_1 Sh_{\beta_1} \end{bmatrix} \begin{Bmatrix} A_1 \\ A_2 \\ A_3 \\ A_4 \end{Bmatrix} = \begin{Bmatrix} 0 \\ 0 \\ 0 \\ 0 \end{Bmatrix}, \quad (24)$$

149 or,

$$\mathbf{R}_x \mathbf{A} = \mathbf{0}, \quad (25)$$

150 where,

$$\begin{aligned} \gamma_1 &= -\alpha_1^3 - \chi^2 \left( \frac{4D_{66}S_3}{D_{11}I_1} - \frac{D_{12}I_2}{D_{11}I_1} \right) \alpha_1, \\ \gamma_2 &= \beta_1^3 - \chi^2 \left( \frac{4D_{66}S_3}{D_{11}I_1} - \frac{D_{12}I_2}{D_{11}I_1} \right) \beta_1, \\ \gamma_3 &= -\alpha_1^2 + \frac{\chi^2 D_{12}I_2}{D_{11}I_1}, \\ \gamma_4 &= \beta_1^2 + \frac{\chi^2 D_{12}I_2}{D_{11}I_1}. \end{aligned} \quad (26)$$

151 Note that the classic boundary conditions can be obtained by selecting ex-  
152 tremely large or small spring stiffness constants. For non-trivial solutions,  
153 the characteristic equation or eigenvalue equation is obtained from the de-  
154 terminant of the matrix  $\mathbf{R}_x$  in Equation (25), which must be zero. However,  
155 solving these transcendental equations is cumbersome and so the DSM is  
156 introduced to avoid such a computation.

157 To develop the plate's dynamic stiffness matrix, with the help of Equa-  
158 tion (9a), the vertical displacement and rotation corresponding to the mode  
159 shape  $\phi(\xi)$  along the  $x$ -direction at edges  $\xi = -1$  and  $\xi = 1$  can be expressed  
160 as:

$$\begin{Bmatrix} \phi_{\xi=-1} \\ \frac{d\phi}{d\xi}_{\xi=-1} \\ \phi_{\xi=1} \\ \frac{d\phi}{d\xi}_{\xi=1} \end{Bmatrix} = \begin{bmatrix} -S_{\alpha_1} & C_{\alpha_1} & -Sh_{\beta_1} & Ch_{\beta_1} \\ \alpha_1 C_{\alpha_1}/a & \alpha_1 S_{\alpha_1}/a & \beta_1 Ch_{\beta_1}/a & -\beta_1 Sh_{\beta_1}/a \\ S_{\alpha_1} & C_{\alpha_1} & Sh_{\beta_1} & Ch_{\beta_1} \\ \alpha_1 C_{\alpha_1}/a & -\alpha_1 S_{\alpha_1}/a & \beta_1 Ch_{\beta_1}/a & \beta_1 Sh_{\beta_1}/a \end{bmatrix} \begin{Bmatrix} A_1 \\ A_2 \\ A_3 \\ A_4 \end{Bmatrix}, \quad (27)$$

161 or,

$$\delta_x = \mathbf{Q}_x \mathbf{A}. \quad (28)$$

162 Solving for the eigenvector  $\mathbf{A}$ , and then substituting into Equation (25), we  
163 obtain:

$$\mathbf{R}_x \mathbf{A} = \mathbf{R}_x \mathbf{Q}_x^{-1} \delta_x = \mathbf{0}. \quad (29)$$

164 where the dynamic stiffness matrix, denoted as  $\mathbf{K}_x = \mathbf{R}_x \mathbf{Q}_x^{-1}$ , can be ob-  
165 tained from Equation (29). This matrix can be used to compute the natural  
166 frequencies of the system instead of solving the eigenvalue equation, and the  
167 method for the computation will be given in Section 3.

## 168 2.2. Dynamic stiffness matrix corresponding to $\omega_y$

169 In this section, the mode shape  $\phi(\xi)$  derived in *Section 2.1* is utilized to  
170 obtain the dynamic stiffness matrix in the  $y$ -direction. The vertical trans-  
171 lational and rotational springs at  $\eta = -1$  are denoted as  $k_{\eta=-1}^v$  and  $k_{\eta=-1}^r$ ,  
172 respectively, while those at  $\eta = 1$  are represented by  $k_{\eta=1}^v$  and  $k_{\eta=1}^r$ .

173 Following the same steps as for the  $x$ -direction, the magnitude of potential  
174 energy of the plate in the  $y$ -direction can be obtained as:

$$\begin{aligned} U = \frac{ab}{2} \int_{-1}^1 & \left[ \frac{D_{11}}{a^4} J_4 \psi^2 + \frac{2D_{12}}{a^2 b^2} J_2 \frac{d^2 \psi}{d\eta^2} \psi + \frac{D_{22}}{b^4} J_1 \left( \frac{d^2 \psi}{d\eta^2} \right)^2 \right. \\ & \left. + \frac{4D_{66}}{a^2 b^2} J_3 \left( \frac{d\psi}{d\eta} \right)^2 \right] d\eta + ab J_1 \left[ \frac{k_{\eta=1}^r}{b^3} \left( \frac{d\psi}{d\eta} \right)^2 + \frac{k_{\eta=1}^v}{b} (\psi)^2 \right]_{\eta=1} \\ & + ab J_1 \left[ \frac{k_{\eta=-1}^r}{b^3} \left( \frac{d\psi}{d\eta} \right)^2 + \frac{k_{\eta=-1}^v}{b} (\psi)^2 \right]_{\eta=-1}, \end{aligned} \quad (30)$$

175 where the integral parameters  $J_1$ ,  $J_2$ ,  $J_3$ , and  $J_4$  are defined and expressed  
176 in Appendix A.

177 The coefficient  $T_0$  of the kinetic energy from Equation (7) for the plate  
178 in the  $y$ -direction can be expressed as:

$$T_0 = \frac{ab}{2} \rho h J_1 \int_{-1}^1 \psi^2 d\eta. \quad (31)$$

179 Take the Rayleigh principle in the form:

$$\delta U = \omega_y^2 \delta T_0. \quad (32)$$

180 By substituting Equations (30) and (31) into Equation (32), and relieving  
 181  $\delta\psi$  and  $\delta\frac{d\psi}{d\eta}$  in Equation (32) by calculus of variation, yields:

$$\begin{aligned}
 0 = & \int_{-1}^1 \left[ \frac{D_{22}}{b^4} J_1 \frac{d^4\psi}{d\eta^4} + \left( \frac{2D_{12}}{a^2b^2} J_2 - \frac{4D_{66}}{a^2b^2} J_3 \right) \frac{d^2\psi}{d\eta^2} \right. \\
 & + \left. \left( \frac{D_{11}}{a^4} J_4 - \omega_y^2 \rho h J_1 \right) \psi \right] \delta\psi d\eta \\
 & + \frac{2k_{\eta=-1}^v}{b} J_1 (\psi \delta\psi)_{\eta=-1} + \frac{2k_{\eta=1}^v}{b} J_1 (\psi \delta\psi)_{\eta=1} \\
 & + \left[ \left( \frac{4D_{66}}{a^2b^2} J_3 - \frac{D_{12}}{a^2b^2} J_2 \right) \frac{d\psi}{d\eta} - \frac{D_{22}}{b^4} J_1 \frac{d^3\psi}{d\eta^3} \right] \delta\psi \Big|_{\eta=-1}^{\eta=1} \\
 & + \left( \frac{D_{12}}{a^2b^2} J_2 \psi + \frac{D_{22}}{b^4} J_1 \frac{d^2\psi}{d\eta^2} \right) \delta \frac{d\psi}{d\eta} \Big|_{\eta=-1}^{\eta=1} \\
 & + \frac{2k_{\eta=-1}^r}{b^3} J_1 \left( \frac{d\psi}{d\eta} \delta \frac{d\psi}{d\eta} \right)_{\eta=-1} + \frac{2k_{\eta=1}^r}{b^3} J_1 \left( \frac{d\psi}{d\eta} \delta \frac{d\psi}{d\eta} \right)_{\eta=1}.
 \end{aligned} \tag{33}$$

182 Thus, the governing differential equation in the  $y$ -direction can be obtained  
 183 from the integration part in Equation (33):

$$\frac{d^4\psi}{d\eta^4} + \frac{2}{\chi^2} \left( \frac{D_{12}J_2}{D_{22}J_1} - 2 \frac{D_{66}J_3}{D_{22}J_1} \right) \frac{d^2\psi}{d\eta^2} + \left( \frac{D_{11}J_4}{\chi^4 D_{22}J_1} - \frac{b^4 D_{11}}{D_{22}} \Omega_y^4 \right) \psi = 0, \tag{34}$$

184 where  $\Omega_y = \sqrt[4]{\omega_y^2 \rho h / D_{11}}$ . By substituting  $\psi(\eta) = Be^{\lambda\eta}$  into Equation (34),  
 185 yields:

$$\lambda^4 + \frac{2}{\chi^2} \left( \frac{D_{12}J_2}{D_{22}J_1} - 2 \frac{D_{66}J_3}{D_{22}J_1} \right) \lambda^2 + \left( \frac{D_{11}J_4}{\chi^4 D_{22}J_1} - \frac{b^4 D_{11}}{D_{22}} \Omega_y^4 \right) = 0. \tag{35}$$

186 The solution for  $\lambda$  can be expressed as:

$$\lambda_{1,2} = \pm i\alpha_2, \quad \lambda_{3,4} = \pm \beta_2, \tag{36}$$

187 where,

$$\alpha_2 = \frac{1}{\chi} \sqrt{\sqrt{\left(\frac{D_{12}J_2}{D_{22}J_1} - 2\frac{D_{66}J_3}{D_{22}J_1}\right)^2 - \frac{D_{11}J_4}{D_{22}J_1} + \frac{a^4 D_{11}}{D_{22}} \Omega_y^4 + \frac{D_{12}J_2}{D_{22}J_1} - 2\frac{D_{66}J_3}{D_{22}J_1}}, \quad (37a)$$

$$\beta_2 = \frac{1}{\chi} \sqrt{\sqrt{\left(\frac{D_{12}J_2}{D_{22}J_1} - 2\frac{D_{66}J_3}{D_{22}J_1}\right)^2 - \frac{D_{11}J_4}{D_{22}J_1} + \frac{a^4 D_{11}}{D_{22}} \Omega_y^4 - \frac{D_{12}J_2}{D_{22}J_1} + 2\frac{D_{66}J_3}{D_{22}J_1}}. \quad (37b)$$

188 The boundary conditions along the edges in the  $y$ -direction can be obtained  
 189 from the remaining  $\delta\psi$  and  $\delta\frac{d\psi}{d\eta}$  parts in Equation (33). The shear force  
 190 equilibrium can be obtained from the  $\delta\psi$  part:

$$\begin{aligned} & \left[ \left( \frac{4D_{66}}{a^2b^2} J_3 - \frac{D_{12}}{a^2b^2} J_2 \right) \frac{d\psi}{d\eta} - \frac{D_{22}}{b^4} J_1 \frac{d^3\psi}{d\eta^3} \right] \Big|_{\eta=-1}^{\eta=1} \\ & + \frac{2k_{\eta=-1}^v}{b} J_1(\psi)_{\eta=-1} + \frac{2k_{\eta=1}^v}{b} J_1(\psi)_{\eta=1} = 0, \end{aligned} \quad (38)$$

191 and from the  $\delta\frac{d\psi}{d\eta}$  part, the bending moment equilibrium:

$$\begin{aligned} & \left( \frac{D_{12}}{a^2b^2} J_2 \psi + \frac{D_{22}}{b^4} J_1 \frac{d^2\psi}{d\eta^2} \right) \Big|_{\eta=-1}^{\eta=1} + \frac{2k_{\eta=-1}^r}{b^3} J_1 \left( \frac{d\psi}{d\eta} \right)_{\eta=-1} \\ & + \frac{2k_{\eta=1}^r}{b^3} J_1 \left( \frac{d\psi}{d\eta} \right)_{\eta=1} = 0. \end{aligned} \quad (39)$$

192 Similarly, from the shear force and bending moment equilibrium, and by  
 193 denoting  $k_{\eta}^{v*} = \frac{2b^3k_{\eta}^v}{D_{22}}$ ,  $k_{\eta}^{r*} = \frac{2bk_{\eta}^r}{D_{22}}$ ,  $S_{\alpha_2} = \sin \alpha_2$ ,  $C_{\alpha_2} = \cos \alpha_2$ ,  $Sh_{\beta_2} = \sinh \beta_2$ ,  
 194 and  $Ch_{\beta_2} = \cosh \beta_2$ , We can obtain:

$$\begin{aligned} & \begin{bmatrix} \zeta_1 C_{\alpha_2} - k_{\eta=-1}^{v*} S_{\alpha_2} & \zeta_1 S_{\alpha_2} + k_{\eta=-1}^{v*} C_{\alpha_2} & \zeta_2 Ch_{\beta_2} - k_{\eta=-1}^{v*} Sh_{\beta_2} \\ \zeta_3 S_{\alpha_2} + k_{\eta=-1}^{r*} \alpha_2 C_{\alpha_2} & -\zeta_3 C_{\alpha_2} + k_{\eta=-1}^{r*} \alpha_2 S_{\alpha_2} & \zeta_4 Sh_{\beta_2} + k_{\eta=-1}^{r*} \beta_2 Ch_{\beta_2} \\ -\zeta_1 C_{\alpha_2} + k_{\eta=1}^{v*} S_{\alpha_2} & \zeta_1 S_{\alpha_2} + k_{\eta=1}^{v*} C_{\alpha_2} & -\zeta_2 Ch_{\beta_2} + k_{\eta=1}^{v*} Sh_{\beta_2} \\ \zeta_3 S_{\alpha_2} + k_{\eta=1}^{r*} \alpha_2 C_{\alpha_2} & \zeta_3 C_{\alpha_2} - k_{\eta=1}^{r*} \alpha_2 S_{\alpha_2} & \zeta_4 Sh_{\beta_2} + k_{\eta=1}^{r*} \beta_2 Ch_{\beta_2} \\ -\zeta_2 Sh_{\beta_2} + k_{\eta=-1}^{v*} Ch_{\beta_2} & -\zeta_4 Ch_{\beta_2} - k_{\eta=-1}^{r*} \beta_2 Sh_{\beta_2} & \\ -\zeta_2 Sh_{\beta_2} + k_{\eta=1}^{v*} Ch_{\beta_2} & \zeta_4 Ch_{\beta_2} + k_{\eta=1}^{r*} \beta_2 Sh_{\beta_2} & \end{bmatrix} \begin{Bmatrix} B_1 \\ B_2 \\ B_3 \\ B_4 \end{Bmatrix} = \begin{Bmatrix} 0 \\ 0 \\ 0 \\ 0 \end{Bmatrix}, \end{aligned} \quad (40)$$

195 or,

$$\mathbf{R}_y \mathbf{B} = \mathbf{0}, \quad (41)$$

196 where,

$$\begin{aligned} \zeta_1 &= -\alpha_2^3 - \left( \frac{4D_{66}J_3}{\chi^2 D_{22}J_1} - \frac{D_{12}J_2}{\chi^2 D_{22}J_1} \right) \alpha_2, \\ \zeta_2 &= \beta_2^3 - \left( \frac{4D_{66}T_3}{\chi^2 D_{22}J_1} - \frac{D_{12}J_2}{\chi^2 D_{22}J_1} \right) \beta_2, \\ \zeta_3 &= -\alpha_2^2 + \frac{D_{12}J_2}{\chi^2 D_{22}J_1}, \\ \zeta_4 &= \beta_2^2 + \frac{D_{12}J_2}{\chi^2 D_{22}J_1}. \end{aligned} \quad (42)$$

197 With the help of Equation (9b), the vertical displacement and rotation cor-  
 198 responding to the mode shape  $\psi$  along the  $y$ -direction at the edges  $\eta = -1$   
 199 and  $\eta = 1$  can be expressed as:

$$\begin{Bmatrix} \psi_{\eta=-1} \\ \frac{d\psi}{d\eta}_{\eta=-1} \\ \psi_{\eta=1} \\ \frac{d\psi}{d\eta}_{\eta=1} \end{Bmatrix} = \begin{bmatrix} -S_{\alpha_2} & C_{\alpha_2} & -Sh_{\beta_2} & Ch_{\beta_2} \\ \alpha_2 C_{\alpha_2}/b & \alpha_2 S_{\alpha_2}/b & \beta_2 Ch_{\beta_2}/b & -\beta_2 Sh_{\beta_2}/b \\ S_{\alpha_2} & C_{\alpha_2} & Sh_{\beta_2} & Ch_{\beta_2} \\ \alpha_2 C_{\alpha_2}/b & -\frac{\alpha_2 S_{\alpha_2}}{b} & \beta_2 Ch_{\beta_2}/b & \beta_2 Sh_{\beta_2}/b \end{bmatrix} \begin{Bmatrix} B_1 \\ B_2 \\ B_3 \\ B_4 \end{Bmatrix}, \quad (43)$$

200 or,

$$\delta_y = \mathbf{Q}_y \mathbf{B}. \quad (44)$$

201 Solving for the eigenvector  $\mathbf{B}$ , and then substituting into Equation (41), we  
 202 obtain:

$$\mathbf{R}_y \mathbf{B} = \mathbf{R}_y \mathbf{Q}_x^{-1} \delta_y = \mathbf{0}, \quad (45)$$

203 where the dynamic stiffness matrix, denoted as  $\mathbf{K}_y = \mathbf{R}_y \mathbf{Q}_y^{-1}$ , can be ob-  
 204 tained from Equation (45).

### 205 3. Frequency and mode shape computation

#### 206 3.1. Wittrick-Williams algorithm and enhancement

207 The Wittrick-Williams (W-W) algorithm [23] is an effective method for  
 208 determining the natural frequencies from the dynamic stiffness matrix with

209 high reliability. Instead of directly solving the equations, the algorithm com-  
 210 putes the total number  $J$  of natural frequencies below a given frequency  $\omega^*$ ,  
 211 which is represented as:

$$J(\omega^*) = J_0(\omega^*) + s\{\mathbf{K}^\Delta(\omega^*)\} = J_0(\omega^*) + J_k(\omega^*), \quad (46)$$

212 where  $J_0$  represents the number of natural frequencies of the structure with  
 213 all ends fully clamped,  $\mathbf{K}^\Delta$  is the upper triangular matrix obtained from the  
 214 dynamic stiffness matrix  $\mathbf{K}$  after applying Gaussian elimination, and  $J_k(\omega^*)$   
 215 denotes the number of negative elements in the leading diagonal of  $\mathbf{K}^\Delta$ .

216 It should be noted that the  $J_0$  count is a crucial aspect when applying the  
 217 W-W algorithm. Many previous studies use a sufficiently fine mesh or enough  
 218 terms in series expansions to capture all fully clamped natural frequencies,  
 219 ensuring computational accuracy [1]. However, this approach can make the  
 220 application process cumbersome. To address this issue, the fully clamped  
 221 problem can be replaced with a simply supported problem, where the Navier  
 222 solution for the simply supported plate is used to count  $J_0$  [18]. Nevertheless,  
 223 since analytical solutions in DSM methods involve an infinite series of Fourier  
 224 terms, a sufficient number of truncation terms is required to ensure accuracy  
 225 and convergence.

226 In fact,  $J_0$  can be indirectly determined by evaluating the number of  
 227 natural frequencies  $J$  of the structure under specific boundary conditions,  
 228 which are generally different from the original boundary conditions [8]:

$$J_0(p_1, \omega^*) = J(\bar{p}_1, \omega^*) - J_k(\bar{p}_1, \omega^*), \quad (47)$$

229 where  $p_1$  denotes the fully clamped supports, and  $\bar{p}_1$  denotes specific sup-  
 230 ports, which are typically simply supported, guided, or a combination of the  
 231 two. For these specific boundary conditions, the eigenvalue equations of SOV  
 232 type solution take the form of a single harmonic function. By substituting  
 233 Equation (47) into Equation (46) we get the algorithm as:

$$J(p, \omega^*) = J(\bar{p}_1, \omega^*) - J_k(\bar{p}_1, \omega^*) + J_k(p, \omega^*) \quad (48)$$

234 where  $p$  represents the original boundary conditions of the structure. There-  
 235 fore, the challenge of determining  $J_0(p_1, \omega^*)$  can be transformed into the  
 236 problem of solving  $J(\bar{p}_1, \omega^*)$  instead.

237 By taking fully simply supported boundary conditions as the example,  
 238 the eigenvalue equation corresponding to the natural frequency parameter

239  $\Omega_x$  can be obtained from the determinant of the coefficient matrix  $\mathbf{R}_x$  in  
 240 Equation (24), as given by:

$$\sin 2\alpha_1 = 0. \quad (49)$$

241 With the help of Equations (20a) and (49), the closed-form solution of the  
 242  $n_x$ -th simply supported frequency  $\Omega_{x,n_x}$  for the given  $n_y$ -order  $\psi_{n_y}(\eta)$  can be  
 243 expressed as:

$$\begin{aligned} b\Omega_{x,n_x}^4 = & \left[ \left( \frac{n_x \pi}{2\chi} \right)^2 - \frac{D_{12}S_2}{D_{11}S_1} + 2\frac{D_{66}S_3}{D_{11}S_1} \right]^2 \\ & - \left( \frac{D_{12}S_2}{D_{11}S_1} - 2\frac{D_{66}S_3}{D_{11}S_1} \right)^2 + \frac{D_{22}S_4}{D_{11}S_1}. \end{aligned} \quad (50)$$

244 For  $\Omega_{x,n_x} \leq \Omega_x^* < \Omega_{x,n_x+1}$ ,  $J(\bar{p}_1, \Omega_x^*) = n_x$ . Similarly, the closed-form solution  
 245 of the  $n_y$ -th simply supported frequency  $\Omega_{y,n_y}$  for the given  $n_x$ -order  $\phi_{n_x}(\xi)$   
 246 can be expressed as:

$$\begin{aligned} a\Omega_{y,n_y}^4 = & \frac{D_{22}}{D_{11}} \left\{ \left[ \left( \frac{n_y \pi \chi}{2} \right)^2 - \frac{D_{12}T_2}{D_{22}T_1} + 2\frac{D_{66}T_3}{D_{22}T_1} \right]^2 \right. \\ & \left. - \left( \frac{D_{12}T_2}{D_{22}T_1} - 2\frac{D_{66}T_3}{D_{22}T_1} \right)^2 + \frac{D_{11}T_4}{D_{22}T_1} \right\}. \end{aligned} \quad (51)$$

247 For  $\Omega_{y,n_y} \leq \Omega_y^* < \Omega_{y,n_y+1}$ ,  $J(\bar{p}_1, \Omega_y^*) = n_y$ . According to the relationships  
 248  $\Omega_x^4 = \omega_x^2 \rho h / D_{11}$  and  $\Omega_y^4 = \omega_y^2 \rho h / D_{11}$ , the values of  $J(\bar{p}_1, \omega_x^*)$  and  $J(\bar{p}_1, \omega_y^*)$  can  
 249 be derived from  $J(\bar{p}_1, \Omega_x^*)$  and  $J(\bar{p}_1, \Omega_y^*)$ , respectively. Therefore, this refined  
 250 W-W algorithm can be applied to estimate the lower and upper bounds of  
 251 the frequency range, denoted as  $\omega_l$  and  $\omega_u$ , yielding an approximation for the  
 252 frequency  $\omega_a \in (\omega_l, \omega_u)$  to arbitrary precision.

### 253 3.2. Mode shape computation

254 The mode shape coefficients  $A_1$  to  $A_4$  and  $B_1$  to  $B_4$  in the eigenvectors  $\mathbf{A}$   
 255 and  $\mathbf{B}$  for all classic boundary conditions are provided in [27]. Alternatively,  
 256 these coefficients can also be obtained through a simple numerical method,  
 257 which this work presents as an approach. Here, we illustrate solving the  
 258 eigenvector  $\mathbf{A}$  as an example. By assuming the exact natural frequency as  
 259  $\omega_k$ , we can expand the coefficient matrix  $\mathbf{R}_x$  in Equation (24) using a first-  
 260 order Taylor series about  $\omega_a$ :

$$\mathbf{R}_{x,k}(\omega_k)\mathbf{A}_k = \mathbf{R}_{x,a}\mathbf{A}_k + (\omega_k - \omega_a)\mathbf{R}'_{x,a}\mathbf{A}_k + O((\omega_k - \omega_a)^2) = 0. \quad (52)$$



261 Ignoring higher-order terms, an eigenvalue problem can be derived from  
 262 Equation (52):

$$(\mathbf{R}'_{x,a})^{-1} \mathbf{R}_{x,a} \mathbf{A} = (\omega_a - \omega_k) \mathbf{A} = \tau \mathbf{A}. \quad (53)$$

263 This eigenvalue problem can be solved using the inverse iteration procedure  
 264 [30]:

$$\bar{\mathbf{A}}^{(i+1)} = \mathbf{R}_{x,a}^{-1} \mathbf{R}'_{x,a} \mathbf{A}^{(i)}, \quad (54)$$

265 where the initial guess for  $\mathbf{A}^{(0)}$  is a column vector consisting of four randomly  
 266 generated elements, each of which falls within the range (0,1). The updated  
 267 eigenvalue for the next step can be obtained as:

$$\tau^{(i+1)} = \frac{1}{\bar{A}_j^{(i+1)}}, \quad (55)$$

268 where,

$$|\bar{A}_j^{(i+1)}| = \max(|\bar{A}_1^{(i+1)}|, |\bar{A}_2^{(i+1)}|, |\bar{A}_3^{(i+1)}|, |\bar{A}_4^{(i+1)}|). \quad (56)$$

269 The updated eigenvector can be obtained as:

$$\mathbf{A}^{(i+1)} = \tau^{(i+1)} \bar{\mathbf{A}}^{(i+1)}. \quad (57)$$

270 The procedure can be controlled by the error tolerance  $\epsilon$  or maximum allowed  
 271 steps  $i_{\max}$ :

$$\max |A_n^{(i+1)} - A_n^{(i)}| < \epsilon, \quad (58a)$$

$$i = i_{\max}. \quad (58b)$$

272 Note that the mode shape coefficients  $A_1$  to  $A_4$  obtained from  $\mathbf{A}^{(i+1)}$  are  
 273 applied for the elastically restrained boundary conditions.

### 274 3.3. Application procedure

275 The procedure of the proposed method is as follows:

- 276 • **Step 1** Assume initial integral parameters  $I_1^{(0)}$ ,  $I_2^{(0)}$ ,  $I_3^{(0)}$ , and  $I_4^{(0)}$  in the  
 277  $y$ -direction. Using the given boundary conditions at  $\xi = -1$  and  $\xi = 1$ ,  
 278 determine  $\mathbf{K}_x^{(0)}$  from Equation (29). Then, apply the computational  
 279 algorithms in Section 3.1 to compute the lower and upper bounds of the  
 280  $n_x$ -th non-dimensional frequency parameter,  $2a\Omega_{l,x,n_x}^{(0)}$  and  $2a\Omega_{u,x,n_x}^{(0)}$ ,  
 281 and take the average  $2a\Omega_{x,n_x}^{(0)} = (2a\Omega_{l,x,n_x}^{(0)} + 2a\Omega_{u,x,n_x}^{(0)})/2$  along with its  
 282 corresponding mode shape  $\phi_{n_x}^{(0)}$ , where  $n_x = 1, 2, 3, \dots$

- 283 • **Step 2** Use  $\phi_{n_x}^{(0)}$  as the prescribed mode to determine  $\mathbf{K}_y^{(1)}$  in Equa-  
 284 tion (45), considering the boundary conditions at  $\eta = -1$  and  $\eta = 1$ .  
 285 Apply the computational algorithms to obtain the  $n_y$ -th frequency pa-  
 286 rameter  $2a\Omega_{y,n_y}^{(1)}$  and its corresponding mode shape  $\psi_{n_y}^{(1)}$ , where  $n_y =$   
 287  $1, 2, 3, \dots$ . This completes the first iteration cycle.
- 288 • **Step 3** Use  $\psi_{n_y}^{(1)}$  as the prescribed  $n_y$ -th mode shape in the  $y$ -direction to  
 289 compute  $\mathbf{K}_x^{(1)}$  from Equation (29), then determine the  $n_x$ -th frequency  
 290 parameter  $2a\Omega_{x,n_x}^{(1)}$  and its corresponding mode shape  $\phi_{n_x}^{(1)}$ .
- 291 • **Step 4** Use  $\phi_{n_x}^{(1)}$  as the prescribed mode in the  $x$ -direction to com-  
 292 pute the  $n_y$ -th frequency parameter  $2a\Omega_{y,n_y}^{(2)}$  and its corresponding mode  
 293 shape  $\psi_{n_y}^{(2)}$ , completing the second iteration cycle.
- 294 • **Step 5** Stop the iteration if  $|2a\Omega_{x,n_x}^{(i)} - 2a\Omega_{x,n_x}^{(i+1)}| \leq \Delta 2a\Omega$  or  $|2a\Omega_{y,n_y}^{(i)} -$   
 295  $2a\Omega_{y,n_y}^{(i+1)}| \leq \Delta 2a\Omega$ , where  $\Delta 2a\Omega = 2a\Omega_u - 2a\Omega_l$ . Here,  $2a\Omega_l$  and  $2a\Omega_u$   
 296 are the lower and upper bounds of the frequency parameter range,  
 297 within which the actual frequency parameter  $2a\Omega$  lies, i.e.,  $2a\Omega \in$   
 298  $(2a\Omega_l, 2a\Omega_u)$ . The quantity  $\Delta 2a\Omega$  represents the frequency param-  
 299 eter interval used in the W-W algorithm.
- 300 • **Step 6** Finally, construct the  $(n_x, n_y)$ -th mode shape as  $w(\xi, \eta) =$   
 301  $\phi_{n_x}(\xi)\psi_{n_y}(\eta)$  using Equation (8).

## 302 4. Numerical Results

303 This section presents the numerical validation of the proposed method  
 304 for classic boundary conditions and rotationally restrained boundary con-  
 305 ditions. For all numerical calculations, the initial integral parameters are  
 306 assumed as  $I_1^{(0)} = 1$ ,  $I_2^{(0)} = 1$ ,  $I_3^{(0)} = 1$ , and  $I_4^{(0)} = 10$  in the  $y$ -direction,  
 307 serving as the starting point of **Step 1** for any mode in all boundary con-  
 308 ditions. In this section, the interval between the upper and lower bounds of  
 309 the non-dimensional frequency parameter,  $2a\Delta\Omega$ , is set to 0.005, although  
 310 any desired level of precision can be used. According to our numerical calcu-  
 311 lations, two iteration cycles are generally sufficient to meet the convergence  
 312 requirement (i.e.,  $|2a\Omega_x^{(i)} - 2a\Omega_x^{(i+1)}| \leq \Delta 2a\Omega$  or  $|2a\Omega_y^{(i)} - 2a\Omega_y^{(i+1)}| \leq \Delta 2a\Omega$ )  
 313 for most cases, with at most three cycles required when applying the iterative  
 314 procedure in Section 3.3.

#### 315 4.1. Classical boundary conditions

316 In this subsection, the proposed method is validated by comparison with  
 317 the extended SOV method [27]. The properties of the orthotropic plate,  
 318 consistent with those in [27], are as follows:  $E_1 = 185$  GPa,  $E_2 = 10.5$  GPa,  
 319  $G_{12} = 7.3$  GPa,  $\rho = 1600$  kg m<sup>-1</sup>, and  $\nu_{12} = 0.28$ .

320 The translational springs ( $k^v$ ) and rotational springs ( $k^r$ ) along all edges  
 321 can be set to zero or infinity (represented as  $1 \times 10^{15}$  N m<sup>-1</sup> in the numerical  
 322 calculations of this study) to obtain different classic boundary conditions.

323 The results for SSSS, SCSF, GCGC, CCCC, SSCC, SCCC, GGCC, CCFF,  
 324 CFCF, CFFF, and FFFF boundary conditions are presented in Tables 1 to 3.  
 325 Note that, as is convention, S is a simple support (rotation, no translation),  
 326 C is a clamped supported (no rotation or translation), G is a guided support  
 327 (translation, no rotation), and F is a free edge. These results demonstrate  
 328 high accuracy compared to the extended SOV method, with difference re-  
 329 maining smaller than the frequency parameter interval  $2a\Delta\Omega = 0.005$ . The  
 330 frequency parameters in both directions are equal ( $2a\Omega_x - 2a\Omega_y = 0$ ) in al-  
 331 most all cases, with a few exceptions where  $2a\Omega_x - 2a\Omega_y = 0.005$ . In fact,  
 332 higher accuracy compared to the extended SOV method can be achieved if  
 333 the frequency parameter interval  $2a\Delta\Omega$  is set smaller than 0.005. It should be  
 334 noted that the accuracy improves only by reducing  $2a\Delta\Omega$ , and no additional  
 335 iterations are required according to our calculations. Figure 2 shows the first  
 336 six nonzero mode shapes of a square orthotropic plate with FFFF bound-  
 337 ary conditions, where the mode shape coefficients are calculated using the  
 338 numerical method developed in this study. Instead of selecting fixed expres-  
 339 sions for the mode shape coefficients based on specific boundary conditions,  
 340 our method is applicable to all boundary conditions.

#### 341 4.2. Rotational spring-supported edges

342 In this subsection, rectangular orthotropic plates with rotational spring-  
 343 supported edges with no translations ( $k_\xi^v = k_\eta^v = \infty$ ) are examined. The  
 344 rotational stiffness coefficients are defined as:

$$r_\xi = \frac{2ak_\xi^r}{D_{11}}, \quad (59a)$$

$$r_\eta = \frac{2bk_\eta^r}{D_{22}}. \quad (59b)$$

345 The first example considers a square isotropic plate with all four edges ro-  
 346 tationally restrained. The vertical translational springs along the four edges

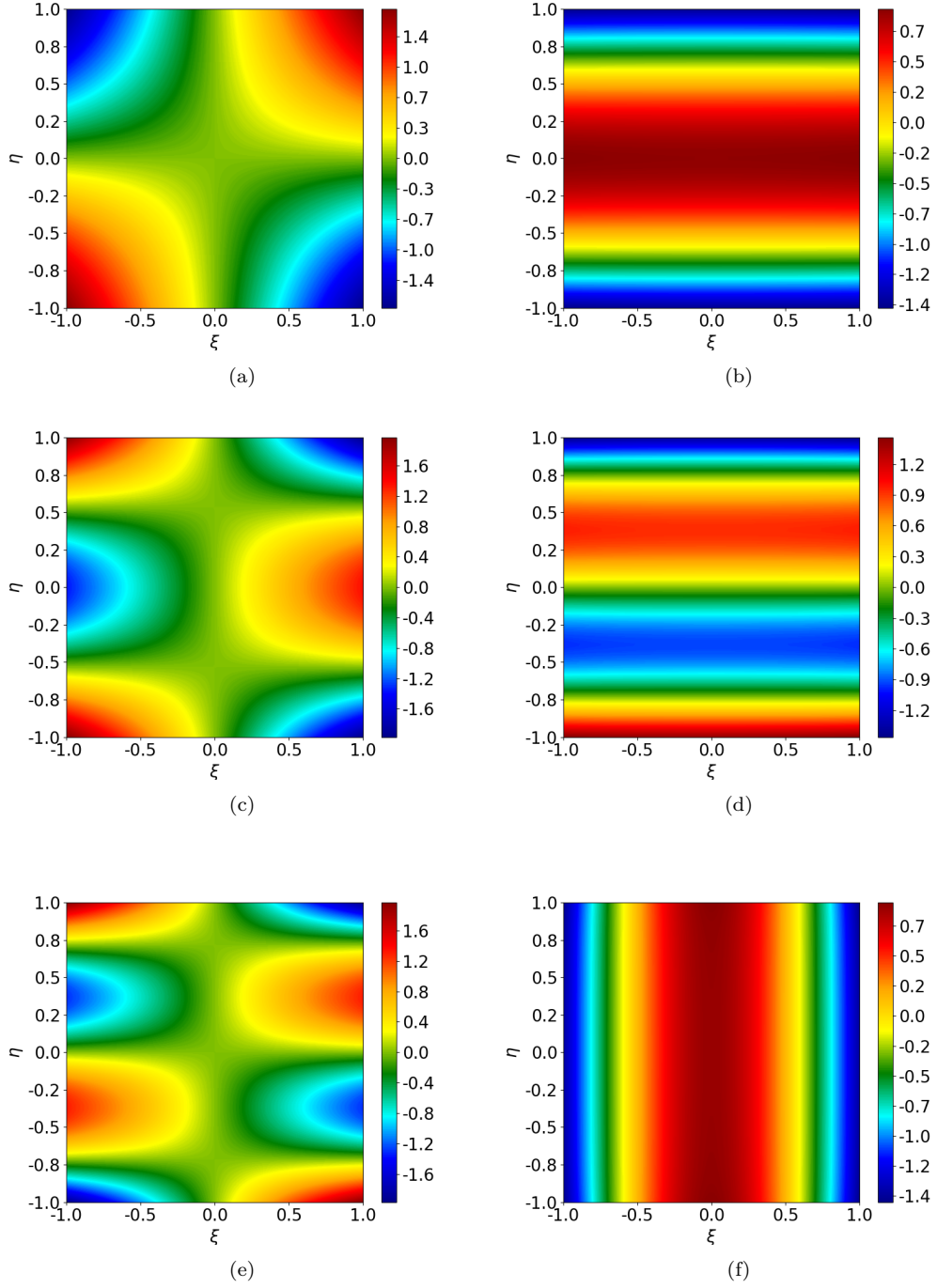


Figure 2: The first six nonzero mode shapes of a square orthotropic plate with FFFF boundary conditions: (a) the first mode; (b) the second mode; (c) the third mode; (d) the fourth mode; (e) the fifth mode; (f) the sixth mode.

Table 1: The first seven frequency parameter  $2a\Omega$  of of orthotropic rectangular plates with SSSS, SCSF and GCGC boundary conditions.

BCs	$\chi$	Mode	$2a\Omega_x = 2a\Omega_y = 2a\sqrt{\rho h\omega^2/D_{11}}$						
			1	2	3	4	5	6	7
SSSS	0.5	Mode number	(1,1)	(1,2)	(1,3)	(1,4)	(1,5)	(1,6)	(1,7)
		extended SOV 27	3.1807	3.3190	3.5938	4.0135	4.5495	5.1635	5.8265
		Present	3.1825	3.3225	3.5975	4.0175	4.5525	5.1625	5.8275
	1	Mode number	(1,1)	(1,2)	(1,3)	(2,1)	(1,4)	(2,2)	(2,3)
		extended SOV 27	3.3190	4.0135	5.1635	6.3615	6.5200	6.6379	7.1876
		Present	3.3175	4.0175	5.1625	6.3625	6.5175	6.6375	7.1875
	1.5	Mode number	(1,1)	(1,2)	(2,1)	(2,2)	(1,3)	(2,3)	(1,4)
		extended SOV 27	3.5938	5.1635	6.4698	7.1876	7.2331	8.5389	9.4352
		Present	3.5975	5.1675	6.4725	7.1875	7.2325	8.5375	9.4375
SCSF	0.5	Mode number	(1,1)	(1,2)	(1,3)	(1,4)	(1,5)	(1,6)	(1,7)
		extended SOV 27	3.1516	3.2451	3.4588	3.8131	4.2950	4.8711	5.5087
		Present	3.1525	3.2475	3.4575	3.8175	4.2925	4.8725	5.5075
	1	Mode number	(1,1)	(1,2)	(1,3)	(1,4)	(2,1)	(2,2)	(2,3)
		extended SOV 27	3.1908	3.6428	4.5972	5.8599	6.3033	6.4901	6.9177
		Present	3.1925	3.6425	4.5975	5.8575	6.3025	6.4925	6.9175
	1.5	Mode number	(1,1)	(1,2)	(1,3)	(2,1)	(2,2)	(2,3)	(1,4)
		extended SOV 27	3.2710	4.3430	6.2157	6.3337	6.8043	7.8718	8.3518
		Present	3.2725	4.3425	6.2175	6.3325	6.8025	7.8725	8.3525
GCGC	0.5	Mode number	(1,1)	(1,2)	(1,3)	(2,1)	(2,2)	(1,4)	(2,3)
		extended SOV 27	1.1544	1.9166	2.6835	3.1983	3.3890	3.4501	3.7372
		Present	1.1525	1.9175	2.6825	3.1975	3.3875	3.4525	3.7375
	1	Mode number	(1,1)	(2,1)	(1,2)	(2,2)	(1,3)	(2,3)	(3,1)
		extended SOV 27	2.3087	3.4900	3.8331	4.4682	5.3669	5.7736	6.3967
		Present	2.3075	3.4875	3.8325	4.4675	5.3675	5.7725	6.3975
	1.5	Mode number	(1,1)	(2,1)	(1,2)	(2,2)	(3,1)	(3,2)	(1,3)
		extended SOV 27	3.4631	4.1353	5.7497	6.0981	6.6049	7.6449	8.0504
		Present	3.4625	4.1325	5.7475	6.0975	6.6075	7.6425	8.0525

Table 2: The first seven frequency parameter  $2a\Omega$  of of orthotropic rectangular plates with CCCC, SSCC, SCCC and GGCC boundary conditions.

BCs	$\chi$	Mode	$2a\Omega_x = 2a\Omega_y = 2a\sqrt{\rho h \omega^2 / D_{11}}$						
			1	2	3	4	5	6	7
CCCC	0.5	Mode number	(1,1)	(1,2)	(1,3)	(1,4)	(1,5)	(1,6)	(1,7)
		extended SOV 27	4.7500	4.8208	4.9682	5.2177	5.5791	6.0430	6.5892
		Present	4.7475	4.8225	4.9725	5.2175	5.5825	6.0425	6.5875
	1	Mode number	(1,1)	(1,2)	(1,3)	(1,4)	(2,1)	(2,2)	(2,3)
		extended SOV 27	4.8579	5.3546	6.2819	7.4972	7.9193	8.1490	8.6054
		Present	4.8575	5.3575	6.2875	7.4975	7.9175	8.1475	8.6075
	1.5	Mode number	(1,1)	(1,2)	(2,1)	(1,3)	(2,2)	(2,3)	(1,4)
		extended SOV 27	5.1581	6.5412	8.0409	8.4945	8.7204	9.9793	10.6460
		Present	5.1575	6.5375	8.0425	8.4975	8.7175	9.9775	10.6425
SSCC	0.5	Mode number	(1,1)	(1,2)	(1,3)	(1,4)	(1,5)	(1,6)	(1,7)
		extended SOV 27	3.9542	4.0520	4.2525	4.5785	5.0254	5.5682	6.1789
		Present	3.9575	4.0525	4.2475	4.5775	5.0225	5.5725	6.1825
	1	Mode number	(1,1)	(1,2)	(1,3)	(1,4)	(2,1)	(2,2)	(2,3)
		extended SOV 27	4.0745	4.6606	5.7009	6.9940	7.1396	7.3894	7.8881
		Present	4.0775	4.6625	5.7025	6.9925	7.1375	7.3875	7.8875
	1.5	Mode number	(1,1)	(1,2)	(2,1)	(1,3)	(2,2)	(2,3)	(1,4)
		extended SOV 27	4.3602	5.8384	7.2531	7.8560	7.9481	9.2515	10.0366
		Present	4.3625	5.8325	7.2525	7.8575	7.9525	9.2525	10.0325
SCCC	0.5	Mode number	(1,1)	(1,2)	(1,3)	(1,4)	(1,5)	(1,6)	(1,7)
		extended SOV 27	3.9596	4.0745	4.3027	4.6606	5.1361	5.7009	6.3271
		Present	3.9575	4.0725	4.3025	4.6625	5.1325	5.7025	6.3325
	1	Mode number	(1,1)	(1,2)	(1,3)	(2,1)	(1,4)	(2,2)	(2,3)
		extended SOV 27	4.1349	4.8478	5.9805	7.1541	7.3192	7.4478	8.0121
		Present	4.1325	4.8475	5.9825	7.1525	7.3175	7.4475	8.0125
	1.5	Mode number	(1,1)	(1,2)	(2,1)	(2,2)	(1,3)	(2,3)	(3,1)
		extended SOV 27	4.5824	6.2766	7.3116	8.1528	8.3705	9.5986	10.3507
		Present	4.5825	6.2775	7.3125	8.1525	8.3725	9.5975	10.3525
GGCC	0.5	Mode number	(1,1)	(1,2)	(1,3)	(1,4)	(1,5)	(1,6)	(1,7)
		extended SOV 27	2.3750	2.4841	2.7895	3.2946	3.9226	4.6123	5.3326
		Present	2.3725	2.4875	2.7925	3.2975	3.9225	4.6075	5.3325
	1	Mode number	(1,1)	(1,2)	(1,3)	(2,1)	(2,2)	(1,4)	(2,3)
		extended SOV 27	2.4290	3.1410	4.4293	5.5202	5.7315	5.8801	6.2606
		Present	2.4325	3.1425	4.4325	5.5225	5.7325	5.8775	6.2625
	1.5	Mode number	(1,1)	(1,2)	(2,1)	(2,2)	(1,3)	(2,3)	(3,1)
		extended SOV 27	2.5790	4.2472	5.5565	6.1533	6.4347	7.5231	8.6732
		Present	2.5825	4.2475	5.5575	6.1525	6.4325	7.5225	8.6725

Table 3: The first seven nonzero frequency parameter  $2a\Omega$  of of orthotropic rectangular plates with CCFF, CFCF, CFFF and FFFF boundary conditions.

BCs	$\chi$	Mode	$2a\Omega_x = 2a\Omega_y = 2a\sqrt{\rho h \omega^2 / D_{11}}$						
			1	2	3	4	5	6	7
CCFF	0.5	Mode number	(1,1)	(1,2)	(1,3)	(1,4)	(1,5)	(1,6)	(2,1)
		extended SOV 27	1.8978	2.0905	2.4925	3.0563	3.7110	4.4117	4.7029
		Present	1.8975	2.0925	2.4925	3.0575	3.7125	4.4125	4.7025
	1	Mode number	(1,1)	(1,2)	(1,3)	(2,1)	(2,2)	(1,4)	(2,3)
		extended SOV 27	1.9930	2.7895	4.0733	4.7338	5.0652	5.5128	5.7419
		Present	1.9925	2.7875	4.0725	4.7325	5.0675	5.5125	5.7425
	1.5	Mode number	(1,1)	(1,2)	(2,1)	(2,2)	(1,3)	(2,3)	(3,1)
		extended SOV 27	2.1780	3.7411	4.7931	5.5758	5.8895	7.0263	7.9006
		Present	2.1775	3.7425	4.7925	5.5725	5.8875	7.0275	7.9025
CFCF	0.5	Mode number	(1,1)	(1,2)	(1,3)	(1,4)	(1,5)	(1,6)	(1,7)
		extended SOV 27	4.7297	4.7427	4.7881	4.8819	5.0478	5.3072	5.6694
		Present	4.7275	4.7425	4.7875	4.8825	5.0475	5.3075	5.6675
	1	Mode number	(1,1)	(1,2)	(1,3)	(1,4)	(1,5)	(1,6)	(2,1)
		extended SOV 27	4.7295	4.7817	5.0012	5.5348	6.4407	7.6182	7.8523
		Present	4.7275	4.7825	5.0025	5.5325	6.4425	7.6175	7.8525
	1.5	Mode number	(1,1)	(1,2)	(1,3)	(1,4)	(2,1)	(2,2)	(2,3)
		extended SOV 27	4.7292	4.8458	5.4221	6.7635	7.8518	7.9470	8.3021
		Present	4.7275	4.8475	5.4225	6.7625	7.8525	7.9475	8.3025
CFFF	0.5	Mode number	(1,1)	(1,2)	(1,3)	(1,4)	(1,5)	(1,6)	(1,7)
		extended SOV 27	1.8751	1.9439	2.1679	2.5657	3.1106	3.7486	4.4382
		Present	1.8775	1.9425	2.1675	2.5675	3.1125	3.7475	4.4375
	1	Mode number	(1,1)	(1,2)	(1,3)	(1,4)	(2,1)	(2,2)	(2,3)
		extended SOV 27	1.8750	2.1242	2.9077	4.1319	4.6937	4.8226	5.2263
		Present	1.8775	2.1225	2.9075	4.1325	4.6925	4.8225	5.2275
	1.5	Mode number	(1,1)	(1,2)	(1,3)	(2,1)	(2,2)	(2,3)	(1,4)
		extended SOV 27	1.8750	2.3402	3.8522	4.6935	4.9753	5.8314	5.9292
		Present	1.8775	2.3425	3.8525	4.6925	4.9775	5.8325	5.9275
FFFF	0.5	Mode number	(1,3)	(2,2)	(1,4)	(2,3)	(1,5)	(2,4)	(2,5)
		extended SOV 27	1.1540	1.4858	1.9157	2.1704	2.6821	2.7881	3.4093
		Present	1.1525	1.4875	1.9175	2.1725	2.6825	2.7875	3.4075
	1	Mode number	(2,2)	(1,3)	(2,3)	(1,4)	(2,4)	(3,1)	(3,2)
		extended SOV 27	2.1311	2.3082	3.2734	3.8320	4.4962	4.7298	4.9138
		Present	2.1325	2.3075	3.2725	3.8325	4.4975	4.7275	4.9125
	1.5	Mode number	(2,2)	(1,3)	(2,3)	(3,1)	(3,2)	(1,4)	(3,3)
		extended SOV 27	2.6277	3.4625	4.2915	4.7296	5.1259	5.7485	6.1588
		Present	2.6275	3.4625	4.2925	4.7275	5.1275	5.7475	6.1575

are numerically set as  $k_{\xi=-1}^v = k_{\xi=1}^v = k_{\eta=-1}^v = k_{\eta=1}^v = 1 \times 10^{12} \text{ N m}^{-1}$ . The material properties are given as  $D_{11} = D_{22} = D_3$  and  $\nu_{12} = \nu_{21} = 0.3$ .

Table 4 presents the frequency parameter  $2a\Omega$  for different rotational stiffness coefficients  $r_\xi = r_\eta$  with values 0.1, 1, 10, 100, and 1000. Notably, when  $r_\xi = r_\eta = 0$  and  $r_\xi = r_\eta = \infty$ , the boundary conditions correspond to SSSS and CCCC, respectively.

Interestingly, the results indicate that the frequencies  $\Omega_x$  and  $\Omega_y$  are not strictly equal for some mode shapes under these boundary conditions. The actual frequency  $\Omega$  lies between  $\Omega_x$  and  $\Omega_y$ , which may be attributed to the fact that  $\Omega_x$  and  $\Omega_y$  satisfy Rayleigh's principle in Equation (3), representing the weak-form governing equations, but do not necessarily satisfy the strong-form governing equations in Equation (1). For a physical problem with exact solutions, both Equations (1) and (3) must be satisfied. If this condition is not met, applying Equation (3) still provides a viable approach for approximating the exact solution of the plate. Thus, the exact frequency can be estimated as  $\Omega = (\Omega_x + \Omega_y)/2$ . As shown in Table 4, the maximum difference between  $\Omega$  and the solutions reported in 31 is less than 1.3%. Figure 3 illustrates the variation in mode shapes corresponding to the fundamental natural frequency as the rotational stiffness  $r_\xi = r_\eta$  increases from zero to  $\infty$ , transitioning the boundary conditions from SSSS to CCCC.

The next example considers a rectangular orthotropic plate with three simply supported edges ( $k_{\xi=-1}^r = k_{\xi=1}^r = k_{\eta=1}^r = 0$ ), while the edge at  $\eta = -1$  is rotationally restrained. The material properties are consistent with those in 31, where  $2D_{11} = 2D_{22} = D_3$  and  $\nu_{12} = \nu_{21} = 0.3$ . Table 5 shows the fundamental frequency results for different length ratios ( $b/a$ ), comparing them with those reported in 31. The maximum observed difference is 0.8% when  $r_{\eta=-1} = 10$ .

Interestingly, in certain numerical calculations involving rotationally restrained boundary conditions, the variables  $\alpha_1$  and  $\alpha_2$  may take complex values rather than being purely real. Consequently, the mode shape coefficients  $A_1$ ,  $A_2$ ,  $B_1$ , and  $B_2$  become complex-valued, leading to  $\mathbf{R}$  and  $\mathbf{Q}^{-1}$  being complex matrices. However, the mode shapes  $\phi(\xi)$  and  $\psi(\eta)$  remain real-valued, and the dynamic stiffness matrix  $\mathbf{K} = \mathbf{R}\mathbf{Q}^{-1}$  is a real symmetric matrix. Thus, the frequency  $\Omega$  can be obtained by solving  $\mathbf{K}$  using the refined W-W algorithm provided in this study, which avoids solving the eigenvalue equations in both the real and complex domains.



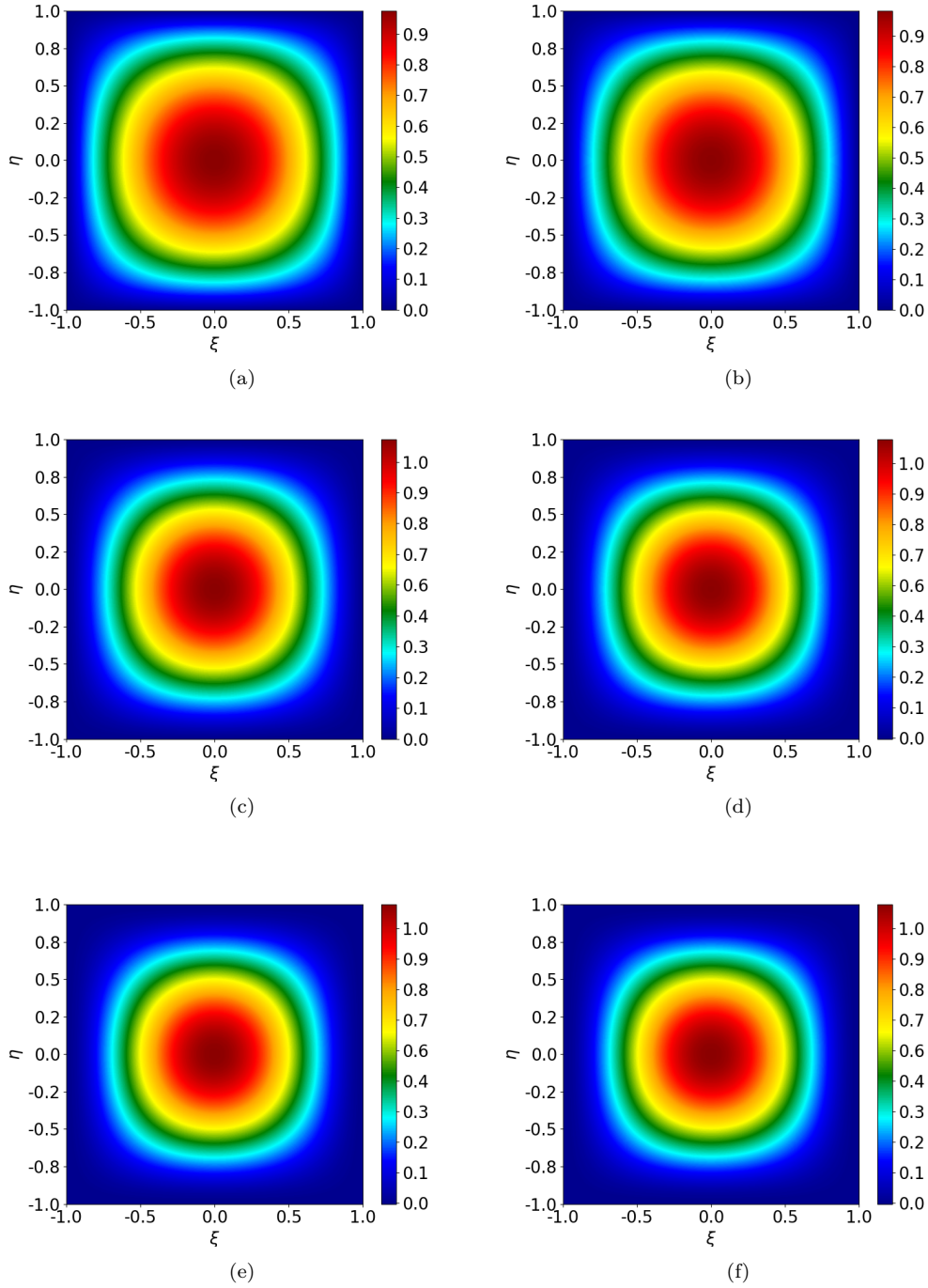


Figure 3: The first mode shape of a square isotropic plate with all four edges rotationally restrained: (a)  $r_\xi = r_\eta = 0$ ; (b)  $r_\xi = r_\eta = 1$ ; (c)  $r_\xi = r_\eta = 10$ ; (d)  $r_\xi = r_\eta = 20$ ; (e)  $r_\xi = r_\eta = 100$ ; (f)  $r_\xi = r_\eta = \infty$ .

Table 4: The first six frequency parameters,  $2a\Omega = 2a\sqrt[4]{\rho h\omega^2/D_{11}}$ , of a square isotropic plate with all four edges rotationally restrained, where  $k_{\xi=-1}^r = k_{\xi=1}^r = k_{\eta=-1}^r = k_{\eta=1}^r$ .

$r$	Mode	$2a\Omega$					
		1	2	3	4	5	6
0.1	Mode number	(1,1)	(1,2)	(2,1)	(2,2)	(1,3)	(3,1)
	Ref.20	4.454	6.992	7.045	8.890	9.782	9.960
	Ref.31	4.465	7.039	7.039	8.897	9.945	9.945
	Present ( $\Omega_x$ )	4.463	7.028	7.043	8.893	9.938	9.953
	Present ( $\Omega_y$ )	4.463	7.043	7.028	8.893	9.953	9.938
	Present ( $\Omega$ )	4.463	7.035	7.035	8.893	9.945	9.945
	Difference (%)	0.044	0.056	0.056	0.044	0.000	0.000
1	Mode number	(1,1)	(1,2)	(2,1)	(2,2)	(3,1)	(1,3)
	Ref.20	4.529	7.008	7.136	8.936	9.787	10.036
	Ref.31	4.637	7.155	7.155	8.991	10.029	10.030
	Present ( $\Omega_x$ )	4.648	7.098	7.223	8.993	10.093	9.968
	Present ( $\Omega_y$ )	4.648	7.223	7.098	8.993	9.968	10.098
	Present ( $\Omega$ )	4.648	7.160	7.160	8.993	10.030	10.033
	Difference (%)	0.237	0.069	0.069	0.022	0.009	0.029
10	Mode number	(1,1)	(1,2)	(2,1)	(2,2)	(1,3)	(3,1)
	Ref.31	5.346	7.768	7.768	9.537	10.552	10.563
	Present ( $\Omega_x$ )	5.413	7.718	7.953	9.598	10.448	10.782
	Present ( $\Omega_y$ )	5.413	7.953	7.718	9.598	10.782	10.453
	Present ( $\Omega$ )	5.413	7.835	7.835	9.598	10.615	10.618
	Difference (%)	1.253	0.862	0.862	0.639	0.597	0.520
100	Mode number	(1,1)	(1,2)	(2,1)	(2,2)	(1,3)	(3,1)
	Ref.20	5.895	8.326	8.422	10.167	10.957	11.297
	Ref.31	5.901	8.442	8.442	10.253	11.307	11.333
	Present ( $\Omega_x$ )	5.913	8.428	8.473	10.258	11.293	11.373
	Present ( $\Omega_y$ )	5.913	8.473	8.478	10.258	11.373	11.293
	Present ( $\Omega$ )	5.913	8.450	8.450	10.258	11.333	11.333
	Difference (%)	0.203	0.094	0.094	0.048	0.229	0.000
1000	Mode number	(1,1)	(1,2)	(2,1)	(2,2)	(1,3)	(3,1)
	Ref.31	6.011	8.585	8.585	10.424	11.495	11.522
	Present ( $\Omega_x$ )	5.988	8.553	8.553	10.388	11.463	11.478
	Present ( $\Omega_y$ )	5.988	8.553	8.553	10.388	11.478	11.463
	Present ( $\Omega$ )	5.988	8.553	8.553	10.388	11.470	11.470
	Difference (%)	0.382	0.372	0.372	0.345	0.217	0.451

Table 5: Fundamental frequency parameter  $2a\Omega = 2a\sqrt[4]{\rho h\omega^2/D_{11}}$  of rectangular orthotropic plates with three edges simply supported ( $k_{\xi=-1}^r = k_{\xi=1}^r = k_{\eta=1}^r = 0$ ) and the edge at  $\eta = -1$  rotationally restrained.

$b/a$	$r_{\eta=-1}$	$2a\Omega$				
		Ref.31	Present ( $\Omega$ )	Present ( $\Omega_x$ )	Present ( $\Omega_y$ )	Difference (%)
0.5	0	7.530	7.523	7.523	7.523	0.092
	1	7.690	7.700	7.588	7.813	0.130
	10	8.250	8.308	8.198	8.418	0.703
	$\infty$	8.705	8.695	8.695	8.695	0.114
1.0	0	4.917	4.918	4.918	4.918	0.020
	1	4.954	4.960	4.933	4.988	0.121
	10	5.114	5.128	5.088	5.168	0.273
	$\infty$	5.289	5.278	5.278	5.278	0.207
1.5	0	4.126	4.128	4.128	4.128	0.048
	1	4.139	4.138	4.128	4.148	0.024
	10	4.202	4.208	4.188	4.228	0.142
	$\infty$	4.292	4.288	4.288	4.288	0.093

## 383 5. Conclusion

384 In this study, the dynamic stiffness matrix (DSM) based on the ex-  
385 tended separation-of-variable (SOV) solution has been developed for the  
386 vibration analysis of an orthotropic rectangular plate with general homo-  
387 geneous boundary conditions.

388 Instead of solving highly nonlinear eigenvalue equations involved in the  
389 SOV methods, the extended SOV solution is adopted to construct the dy-  
390 namic stiffness matrices. Several novel techniques have proposed to solve the  
391 eigenvalue problem and mode shape computation. The challenge of deter-  
392 mining the fully clamped frequencies using the Wittrick–Williams (W–W)  
393 algorithm is resolved by computing the frequencies under specific boundary  
394 conditions, such as simply supported, guided, or a combination of the two,  
395 whose closed-form expression can be easily derived using the SOV method.

396 Classical boundary conditions, such as guided, simply supported, clamped,  
397 and free edges, can be realized by setting the translational springs ( $k^v$ ) and  
398 rotational springs ( $k^r$ ) along the plate edges to either zero or infinity, as  
399 appropriate. Numerical experiments validate the accuracy of this approach  
400 for these boundary conditions. The results shows that the SOV solution can  
401 also be extended to handle elastically-restrained boundary conditions. De-  
402 spite certain approximations inherent in some elastically-restrained cases, the  
403 maximum percentage error across all numerical experiments remains within  
404 1.25%. This may occur because the SOV solution used is derived from the  
405 weak-form governing equation, which is based on Rayleigh’s principle.

406 The SOV solution  $\phi(\xi)\psi(\eta)$  consists of only one single term for each mode  
407 order, unlike the sufficiently truncated Fourier series used in the DSM for  
408 each mode, each eigenvalue solution can be explicitly expressed. Therefore,  
409 dynamic stiffness matrices based on the SOV solution have the minimum  
410 matrix dimension compared to existing DSM methods. This suggests the  
411 potential for constructing lower-dimensional dynamic stiffness matrices for  
412 assembled plate structures than those produced by existing DSM approaches.

413 Finally, the developments reported in this paper should find good ap-  
414 plication with researchers and practitioners interested in the vibration of  
415 generally-supported rectangular orthotropic plates.

## 416 Appendix A Integral parameters

417 The integral parameters  $I_1$ ,  $I_2$ ,  $I_3$ , and  $I_4$  are defined as follows:

$$\begin{aligned}
 I_1 &= \int_0^1 \psi^2 d\eta \\
 &= (B_1^2 + B_2^2 - B_3^2 + B_4^2) + \frac{-B_1^2 + B_2^2}{2\alpha_2} \sin(2\alpha_2) + \frac{B_3^2 + B_4^2}{2\beta_2} \sinh(2\beta_2) \\
 &\quad + \frac{4(\alpha_2 B_2 B_4 + \beta_2 B_1 B_3)}{\alpha_2^2 + \beta_2^2} \sin(\alpha_2) \cosh(\beta_2) \\
 &\quad + \frac{4(-\alpha_2 B_1 B_3 + \beta_2 B_2 B_4)}{\alpha_2^2 + \beta_2^2} \cos(\alpha_2) \sinh(\beta_2).
 \end{aligned}
 \tag{A.1}$$

$$\begin{aligned}
 I_2 &= \int_0^1 \left( \psi \frac{d^2 \psi}{d\eta^2} \right) d\eta \\
 &= \left( -\alpha_2^2 B_1^2 - \alpha_2^2 B_2^2 - \beta_2^2 B_3^2 + \beta_2^2 B_4^2 \right) \\
 &\quad + \frac{\alpha_2(B_1^2 - B_2^2)}{2} \sin(2\alpha_2) + \frac{\beta_2(B_3^2 + B_4^2)}{2} \sinh(2\beta_2) \\
 &\quad + \frac{2(-\alpha_2^2 + \beta_2^2)(\alpha_2 B_2 B_4 + \beta_2 B_1 B_3)}{\alpha_2^2 + \beta_2^2} \sin(\alpha_2) \cosh(\beta_2) \\
 &\quad + \frac{2(-\alpha_2^2 + \beta_2^2)(-\alpha_2 B_1 B_3 + \beta_2 B_2 B_4)}{\alpha_2^2 + \beta_2^2} \cos(\alpha_2) \sinh(\beta_2).
 \end{aligned}
 \tag{A.2}$$

$$\begin{aligned}
 I_3 &= \int_0^1 \left( \frac{d\psi}{d\eta} \right)^2 d\eta \\
 &= \alpha_2^2 B_1^2 + \alpha_2^2 B_2^2 + \beta_2^2 B_3^2 - \beta_2^2 B_4^2 \\
 &\quad + \frac{\alpha_2(B_1^2 - B_2^2)}{2} \sin(2\alpha_2) + \frac{\beta_2(B_3^2 + B_4^2)}{2} \sinh(2\beta_2) \\
 &\quad + \frac{4\alpha_2\beta_2(\alpha_2 B_1 B_3 - \beta_2 B_2 B_4)}{\alpha_2^2 + \beta_2^2} \sin(\alpha_2) \cosh(\beta_2) \\
 &\quad + \frac{4\alpha_2\beta_2(\alpha_2 B_2 B_4 + \beta_2 B_1 B_3)}{\alpha_2^2 + \beta_2^2} \cos(\alpha_2) \sinh(\beta_2).
 \end{aligned}
 \tag{A.3}$$

$$\begin{aligned}
I_4 &= \int_0^1 \left( \frac{d^2\psi}{d\eta^2} \right)^2 d\eta \\
&= \left( \alpha_2^4 B_1^2 + \alpha_2^4 B_2^2 - \beta_2^4 B_3^2 + \beta_2^4 B_4^2 \right) \\
&\quad + \frac{\alpha_2^3 (-B_1^2 + B_2^2)}{2} \sin(2\alpha_2) + \frac{\beta_2^3 (B_3^2 + B_4^2)}{2} \sinh(2\beta_2) \\
&\quad + \frac{4\alpha_2^2 \beta_2^2 (-\alpha_2 B_2 B_4 - \beta_2 B_1 B_3)}{\alpha_2^2 + \beta_2^2} \sin(\alpha_2) \cosh(\beta_2) \\
&\quad + \frac{4\alpha_2^2 \beta_2^2 (\alpha_2 B_1 B_3 - \beta_2 B_2 B_4)}{\alpha_2^2 + \beta_2^2} \cos(\alpha_2) \sinh(\beta_2)
\end{aligned} \tag{A.4}$$

421 The integral parameters  $J_1$ ,  $J_2$ ,  $J_3$ , and  $J_4$  can be obtained by replacing  $B_1$   
422 to  $B_4$  by  $A_1$  to  $A_4$ , respectively, and  $\alpha_2$  and  $\beta_2$  by  $\alpha_1$  and  $\beta_1$ , respectively.

## 423 References

- 424 [1] Banerjee, J., Papkov, S., Liu, X., Kennedy, D., 2015. Dynamic stiffness  
425 matrix of a rectangular plate for the general case. *Journal of Sound and*  
426 *Vibration* 342, 177–199. doi:10.1016/j.jsv.2014.12.031.
- 427 [2] Banerjee, J.R., 1997. Dynamic stiffness formulation for structural el-  
428 ements: a general approach. *Computers & Structures* 63, 101–103.  
429 doi:10.1016/S0045-7949(96)00326-4.
- 430 [3] Biancolini, M.E., Brutti, C., Reccia, L., 2005. Approximate solution for  
431 free vibrations of thin orthotropic rectangular plates. *Journal of Sound*  
432 *and Vibration* 288, 321–344. doi:10.1016/j.jsv.2005.01.005.
- 433 [4] Boscolo, M., Banerjee, J., 2011. Dynamic stiffness elements and their ap-  
434 plications for plates using first order shear deformation theory. *Comput-*  
435 *ers & Structures* 89, 395–410. doi:10.1016/j.compstruc.2010.11.005.
- 436 [5] Fazzolari, F., Boscolo, M., Banerjee, J., 2013. An exact dynamic stiffness  
437 element using a higher order shear deformation theory for free vibration  
438 analysis of composite plate assemblies. *Composite Structures* 96, 262–  
439 278. doi:10.1016/j.compstruct.2012.08.033.
- 440 [6] Ghorbel, O., Casimir, J.B., Hammami, L., Tawfiq, I., Haddar, M., 2015.  
441 Dynamic stiffness formulation for free orthotropic plates. *Journal of*  
442 *Sound and Vibration* 346, 361–375. doi:10.1016/j.jsv.2015.02.020.

- 443 [7] Gorman, D.J., 2005. Free in-plane vibration analysis of rectangular  
444 plates with elastic support normal to the boundaries. *Journal of Sound*  
445 *and Vibration* 285, 941–966. doi:10.1016/j.jsv.2004.09.017.
- 446 [8] Han, F., Dan, D., Cheng, W., Zang, J., 2018. An improved wittrick-  
447 williams algorithm for beam-type structures. *Composite Structures* 204,  
448 560–566. doi:10.1016/j.compstruct.2018.07.108.
- 449 [9] Kantorovich, L.V., Krylov, V.I., 1958. *Approximate Methods of Higher*  
450 *Analysis*. Interscience Publishers, New York.
- 451 [10] Kerr, A.D., 1968. An extension of the kantorovich method. *Quarterly*  
452 *of Applied Mathematics* 26, 219–229. doi:10.1090/qam/99857.
- 453 [11] Khov, H., Li, W.L., Gibson, R.F., 2009. An accurate solution method  
454 for the static and dynamic deflections of orthotropic plates with general  
455 boundary conditions. *Composite Structures* 90, 474–481. doi:10.1016/  
456 j.compstruct.2009.04.020.
- 457 [12] Laura, P.A., Saffell Jr, B.F., 1967. Study of small-amplitude vibrations  
458 of clamped rectangular plates using polynomial approximations. *The*  
459 *Journal of the Acoustical Society of America* 41, 836–839. doi:10.1121/  
460 1.1910414.
- 461 [13] Leissa, A.W., 1973. The free vibration of rectangular plates. *Jour-*  
462 *nal of Sound and Vibration* 31, 257–293. doi:10.1016/S0022-460X(73)  
463 80371-2.
- 464 [14] Levy, M., 1899. Sur l’équilibre élastique d’une plaque rectangulaire.  
465 *Comptes Rendus Acad. Sci. Paris* 129, 535–539.
- 466 [15] Li, R., Zhong, Y., Tian, B., Liu, Y., 2009a. On the finite integral trans-  
467 form method for exact bending solutions of fully clamped orthotropic  
468 rectangular thin plates. *Applied Mathematics Letters* 22, 1821–1827.  
469 doi:10.1016/j.aml.2009.07.003.
- 470 [16] Li, W.L., 2004. Vibration analysis of rectangular plates with general  
471 elastic boundary supports. *Journal of Sound and Vibration* 273, 619–  
472 635. doi:10.1016/S0022-460X(03)00562-5.

- 473 [17] Li, W.L., Zhang, X., Du, J., Liu, Z., 2009b. An exact series solu-  
474 tion for the transverse vibration of rectangular plates with general elas-  
475 tic boundary supports. *Journal of Sound and Vibration* 321, 254–269.  
476 doi:10.1016/j.jsv.2008.09.035.
- 477 [18] Liu, X., Banerjee, J., 2015. An exact spectral-dynamic stiffness  
478 method for free flexural vibration analysis of orthotropic composite  
479 plate assemblies—part i: Theory. *Composite Structures* 132, 1274–1287.  
480 doi:10.1016/j.compstruct.2015.07.020.
- 481 [19] Liu, X., Banerjee, J., 2016. Free vibration analysis for plates with  
482 arbitrary boundary conditions using a novel spectral-dynamic stiff-  
483 ness method. *Computers & Structures* 164, 108–126. doi:10.1016/  
484 j.compstruc.2015.11.005.
- 485 [20] Mukhopadhyay, M., 1979. Free vibration of rectangular plates with  
486 edges having different degrees of rotational restraint. *Journal of Sound*  
487 *and Vibration* 67, 459–468.
- 488 [21] Navier, L., 1823. Extrait des recherches sur la flexion des plans elas-  
489 tiques. *Bull. Sci. Soc. Philomat.* , 95–102.
- 490 [22] Timoshenko, S., 1940. *Theory of Plates and Shells*. McGraw-Hill Book  
491 Company.
- 492 [23] Wittrick, W.H., Williams, F.W., 1971. A general algorithm for comput-  
493 ing natural frequencies of elastic structures. *The Quarterly Journal of*  
494 *Mechanics and Applied Mathematics* 24, 263–284. doi:10.1093/qjmam/  
495 24.3.263.
- 496 [24] Xing, Y., Li, G., Yuan, Y., 2022. A review of the analytical solution  
497 methods for the eigenvalue problems of rectangular plates. *International*  
498 *Journal of Mechanical Sciences* 221, 107171. doi:10.1016/j.ijmecsci.  
499 2022.107171.
- 500 [25] Xing, Y., Liu, B., 2009a. New exact solutions for free vibrations of  
501 rectangular thin plates by symplectic dual method. *Acta Mechanica*  
502 *Sinica* 25, 265–270. doi:10.1007/s10409-008-0208-4.
- 503 [26] Xing, Y., Sun, Q., Liu, B., Wang, Z., 2018. The overall assessment  
504 of closed-form solution methods for free vibrations of rectangular thin



- 505 plates. International Journal of Mechanical Sciences 140, 455–470.  
506 doi:10.1016/j.ijmecsci.2018.03.013.
- 507 [27] Xing, Y., Wang, Z., 2020a. An extended separation-of-variable method  
508 for the free vibration of orthotropic rectangular thin plates. International  
509 Journal of Mechanical Sciences 182, 105739. doi:10.1016/j.ijmecsci.  
510 2020.105739.
- 511 [28] Xing, Y., Wang, Z., 2020b. An improved separation-of-variable method  
512 for the free vibration of orthotropic rectangular thin plates. Composite  
513 Structures 252, 112664. doi:10.1016/j.compstruct.2020.112664.
- 514 [29] Xing, Y.F., Liu, B., 2009b. New exact solutions for free vibrations of  
515 thin orthotropic rectangular plates. Composite Structures 89, 567–574.  
516 doi:10.1016/j.compstruct.2008.11.010.
- 517 [30] Yuan, S., Ye, K., Williams, F., 2004. Second order mode-finding method  
518 in dynamic stiffness matrix methods. Journal of Sound and Vibration  
519 269, 689–708. doi:10.1016/S0022-460X(03)00126-3.
- 520 [31] Zhang, S., Xu, L., Li, R., 2019. New exact series solutions for transverse  
521 vibration of rotationally-restrained orthotropic plates. Applied Mathe-  
522 matical Modelling 65, 348–360. doi:10.1016/j.apm.2018.08.033.
- 523 [32] Zhong, W.X., 1995. A new systematic methodology for theory of elas-  
524 ticity. Dalian University of Technology Press, Dalian , 182–187.
- 525 [33] Zhong, Y., Zhao, X.F., Li, R., 2013. Free vibration analysis of rectangu-  
526 lar cantilever plates by finite integral transform method. International  
527 Journal for Computational Methods in Engineering Science and Me-  
528 chanics 14, 221–226. doi:10.1080/15502287.2012.711424.